



Late-orogenic backfolding and extension in the Brooks Range collisional orogen, northern Alaska

James J. Vogl*

Department of Geological Sciences, University of California, Santa Barbara, CA 93106, USA

Received 20 December 2000; revised 10 July 2001; accepted 6 August 2001

Abstract

New structural observations across a crustal section spanning relatively unmetamorphosed fold–thrust belt rocks and epidote–amphibolite grade rocks document the late-orogenic kinematic history of the Brooks Range, Alaska, and provide insight into the character, relative timing, and geodynamic setting of late-orogenic backfolding and extension in collisional orogens. Greenschist-grade rocks on the north flank of a metamorphic culmination display mesoscopic, open-to-close, S-vergent folds (and associated cleavages) and small-displacement normal faults, suggesting a sequence of D_2 backfolding and D_3 extension following the protracted phase of N-directed D_1 . At deeper levels, epidote–amphibolite facies rocks display a pervasive gently N-dipping S_2 crenulation cleavage that is axial-planar to kilometer- and smaller-scale tight to isoclinal recumbent F_2 folds. Porphyroblast–matrix relationships suggest that folds at the deeper levels initiated during synmetamorphic D_2 backfolding. Much of the strain recorded by S_2 and the tightening of folds, however, probably accumulated during post-metamorphic D_3 extension.

$^{40}\text{Ar}/^{39}\text{Ar}$ data suggest an early- to mid-Albian age for D_2 backfolding, which may be related to formation of a regional-scale backfold. Backfolding, together with apparently synchronous thrusting near the range front may represent the final stages of Cretaceous contractional deformation in the orogen. Contraction was immediately followed by extension, which, aided by erosion, produced a short-lived period of cooling and exhumation beginning at ~ 103 Ma. The available data suggest that extension is post-contractional, and thus is not viewed as a driving force of thrusting in the foreland. Extension was not limited to range-bounding normal faults, but rather was distributed over much of the southern half of the Brooks Range, with character of extensional fabrics being dependent on the geometry of D_2 fabrics.

Inasmuch as backfolding and extension are common features within collisional orogenic belts, the conclusions drawn here have implications regarding fundamental processes associated with the late-stages of collisional orogenesis. In particular, the study provides an example of the roles that backfolding and extension have played in the geodynamic development of a collisional orogen. © 2002 Elsevier Science Ltd. All rights reserved.

Keywords: Brooks Range; Extension; Backfolding; Collisional orogenesis; Structural geology

1. Introduction

The late stages of collisional orogenesis are commonly characterized by reversals in the transport direction of thrusts and fold nappes (backfolding) and by the onset of horizontal extension (e.g. Milnes et al., 1981; Dewey, 1988; Parrish et al., 1988; Carmignani and Kligfield, 1990; Escher et al., 1993; Malavieille, 1993; Fossen and Holst, 1995; Anderson, 1998). Although conceptual, numerical, and physical models (e.g. Davis et al., 1983; Stockmal, 1983; Platt, 1986; Koons, 1990; Beaumont et al., 1996; Gutscher et al., 1996, 1998; Escher and Beaumont, 1997) have been used successfully to explain some of the general features of

collisional orogens, many aspects of the roles that backfolding and extension play in the growth and destruction of collisional mountain belts remain conceptual and poorly documented.

The roles of backfolding and extension in collisional orogenesis were investigated in the Brooks Range, which is interpreted to be the result of continent/island-arc collision (e.g. Mayfield et al., 1988; Moore et al., 1994). Previous work has revealed evidence for both backfolding and extension (e.g. Mull, 1978; Carlson, 1985; Gottschalk and Oldow, 1988; Miller and Hudson, 1991), however, these features are poorly documented compared with the dominant foreland-directed contractional phase of deformation. Ambiguities concerning the character, timing, and spatial distribution of these late-orogenic features have led to widely varying models for the late-orogenic mid-Cretaceous evolution of the Brooks Range. For example, current models

* Now at Department of Geology, University of Florida, Gainesville, FL 32611, USA. Tel./fax: +1-904-230-8286.

E-mail address: jvogl@geology.ufl.edu (J.J. Vogl).

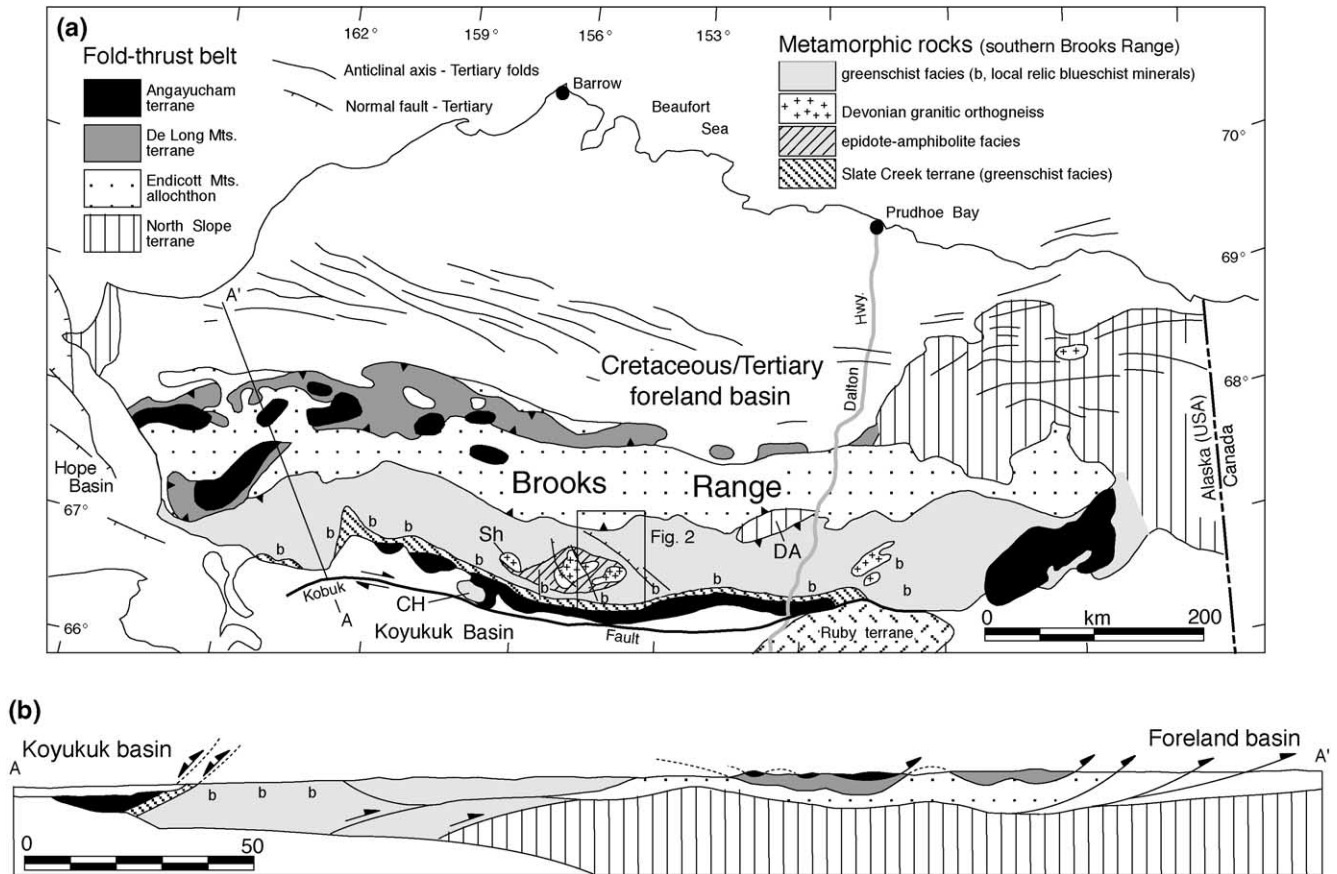


Fig. 1. (a) Terrane and metamorphic map of northern Alaska. CH = Cosmos Hills, DA = Doonarak antiform, SH = Shishakshinovik orthogneiss. Modified from Moore et al. (1997). Tertiary folds from Mull (1985). (b) Simplified cross-section through western Brooks Range. Modified from Moore et al. (1994).

range from lithospheric-scale extension over the interval 130–90 Ma (Miller and Hudson, 1991) to N-directed thrusting in the metamorphic core around 110–105 Ma (Patrick et al., 1994) perhaps accompanied by upper crustal extension (Gottschalk and Oldow, 1988; Gottschalk et al., 1998), to gravitational collapse of the metamorphic core driving thrust faults in the foreland (Toro, 1998).

The goals of this paper are two-fold. The primary goal is to reconstruct the poorly documented, much-debated, late-orogenic kinematic history of the southern Brooks Range. Most of the data presented here document structural fabric sequences, porphyroblast–matrix relationships, and structural style changes across a N-dipping section spanning the relatively unmetamorphosed fold–thrust belt to epidote–amphibolite grade rocks of the metamorphic core. The fabrics and structures described here are some of the youngest associated with Jurassic–Cretaceous orogenesis, thus allowing a more direct approach to the study of late-orogenic deformation than is afforded in many other regions of the Brooks Range. $^{40}\text{Ar}/^{39}\text{Ar}$ data from Vogl et al. (2002) are incorporated to provide age constraints for the deformational events. The second goal of the paper is to use the kinematic and age data from the study area to establish the character, spatial distribution, and relative

timing of backfolding and extension on the orogen scale and to investigate the geodynamic development of the Brooks Range.

Observations and conclusions presented here provide a more complete understanding of the tectonic evolution of the Brooks Range. The study also provides an example of the roles that backfolding and extension have played in the geodynamic development of a collisional orogen.

2. Tectonic setting of the Brooks Range

The Brooks Range orogenic belt has been interpreted to consist of a number of stacked and imbricated allochthons/terrane (Fig. 1), which, when stratigraphically restored, suggest a minimum of 250–600 km of N–S shortening (Mull, 1982; Oldow et al., 1987; Mayfield et al., 1988; Moore et al., 1994, 1997). The structurally highest (Angayucham) terrane consists of a package of dominantly ultramafic and gabbroic rocks that structurally overlie imbricated basaltic and sedimentary rocks, which are believed to represent fragments of an ocean basin that once separated the Alaskan continental margin from the Koyukuk arc to the south (e.g. Patton and Box, 1989;

Moore et al., 1994). The Angayucham terrane is exposed in fault slivers along the south flank of the range and as klippen in the western part of the fold–thrust belt, where it overlies allochthonous sedimentary packages representing various facies of the continental margin (Fig. 1). Allochthons are stacked such that the more distal facies are exposed in the structurally higher allochthons (Mayfield et al., 1988; Moore et al., 1994).

The northern half of the fold–thrust belt is dominated by Devonian to Lower Cretaceous sedimentary rocks of the Endicott Mountains allochthon (EMA), which is internally shortened and defines an open synclinorium that spans most of the length of the Brooks Range (Fig. 1). The EMA is inferred to have been thrust northward by at least 80 km (e.g. Adams et al., 1997) over the parautochthonous North Slope subterrane, which is exposed near the range front and probably within the Doonerak antiform (e.g. Mull et al., 1989; Adams et al., 1997). Along much of its length, including the study area, the EMA structurally overlies more highly strained and metamorphosed rocks whose original paleogeographic position is less clear (Figs. 1a, 2 and 3). Locally, in the western Brooks Range, however, the southern margin of the EMA is structurally overlain by these rocks (Fig. 1b). Generally, rocks south of the EMA consist of a greenschist-grade belt and a more southerly greenschist-overprinted blueschist belt (Fig. 1) that is distinguished by local occurrences of relics and pseudomorphs of Na-amphibole and lawsonite (e.g. Nelson and Grybeck, 1981; Dusel-Bacon et al., 1989). Within the south-central part of the range, an anomalously high-grade region of epidote–amphibolite facies rocks occurs near Devonian granitic orthogneiss bodies (Fig. 1). In the study area, these epidote–amphibolite facies rocks form a metamorphic culmination that is flanked by greenschist–facies and lower-grade rocks (Vogl, 2000).

Most of the shortening in the Brooks Range occurred in the Late Jurassic to Early Cretaceous (e.g. Moore et al., 1994). This phase of deformation (generally referred to as D_1) has produced relatively well-documented, N-directed structures in both the fold–thrust belt and metamorphic core. The timing of the initial northward thrusting is poorly constrained. Middle Jurassic thrust initiation has been suggested by complex $^{40}\text{Ar}/^{39}\text{Ar}$ hornblende data from the metamorphic sole beneath the ophiolite klippe (Wirth et al., 1993). On the basis of Rb–Sr ages (Armstrong et al., 1986), K–Ar dates (Turner et al., 1979) and a single $^{40}\text{Ar}/^{39}\text{Ar}$ plateau age (Christiansen and Snee, 1994), a Middle to Late Jurassic age is also often inferred for the blueschist–facies metamorphism; however, the data are not compelling. Contraction in the fold–thrust belt may have ended in the Albian (Cole et al., 1997). Renewed N–S contraction, however, is thought to have occurred in the latest Cretaceous to Paleocene (e.g. Mull, 1982; O’Sullivan et al., 1995, 1998) and has continued to the present in the north-eastern Brooks Range (Estabrook et al., 1988).

Thrust loading of the continental margin is recorded

by locally highly deformed Neocomian flysch foredeep deposits (Okpikruak Fm.) exposed in allochthons near the northern Brooks Range front (Mull, 1985; Mayfield et al., 1988). Neocomian deposits are overlain by a less deformed Albian to Cenomanian flysch-to-molasse transition sequence, which locally reaches a thickness of ~6 km (Mull, 1985; Moore et al., 1994). In the Koyukuk basin south of the Brooks Range (Fig. 1), deep-water early Albian flysch/molasse that overlie Valanginian shallow-water volcanogenic sedimentary rocks, record Hauterivian to Aptian subsidence and erosional unroofing of the Brooks Range (Dillon, 1989; Nilsen, 1989).

On the south flank of the Brooks Range, blueschist/greenschist–facies rocks are separated from lower grade basalts of the Angayucham terrane by extensional faults and shear zones (e.g. Carlson, 1985; Gottschalk and Oldow, 1988; Law et al., 1994; Little et al., 1994). Whether these faults are the result of lithospheric-scale extensional collapse (Miller and Hudson, 1991), or a response to thickening by deeper level thrusting (Gottschalk and Oldow, 1988) remains a matter of debate, as does the role of extension in producing ductile fabrics preserved north of the extensional fault zone (cf. Law et al., 1994; Patrick et al., 1994; Dinklage, 1998; Gottschalk et al., 1998; Toro, 1998). The extensional faulting has not been dated directly and will be discussed in a later section.

3. Overview of the study area

Map- and smaller scale relations were determined along a N–S transect in the Alatna River region near cross-section A–A' of Fig. 2. Reconnaissance traverses were also done along various parts of the Alatna River to better understand the structures of the study area in terms of the larger scale structural framework. Previously, the area was mapped at 1:250,000 scale by Nelson and Grybeck (1980).

The study area lies on the north flank of an epidote–amphibolite facies metamorphic culmination and comprises a ~10-km-thick, gently N-dipping structural section (Figs. 2 and 3). Constraints on peak metamorphic pressure–temperature conditions (Vogl, 2000) are shown in Fig. 3. For discussion, the area is divided into two domains representing different structural levels that are juxtaposed across the steeply NE-dipping Tertiary (?) Takahula Fault, with apparent NE-side down offset. The epidote–amphibolite facies rocks south of the Takahula Fault are referred to as the metamorphic core (Figs. 2 and 3), whereas the greenschist–grade rocks north of the fault are referred to as the transition zone (Figs. 2 and 3) because metamorphic grade and magnitude of penetrative strain in these rocks are intermediate between the overlying rocks of the fold–thrust belt and those of the metamorphic core.

The highest levels observed in this study consist of Late Devonian Noatak Sandstone (correlation from G. Mull, oral

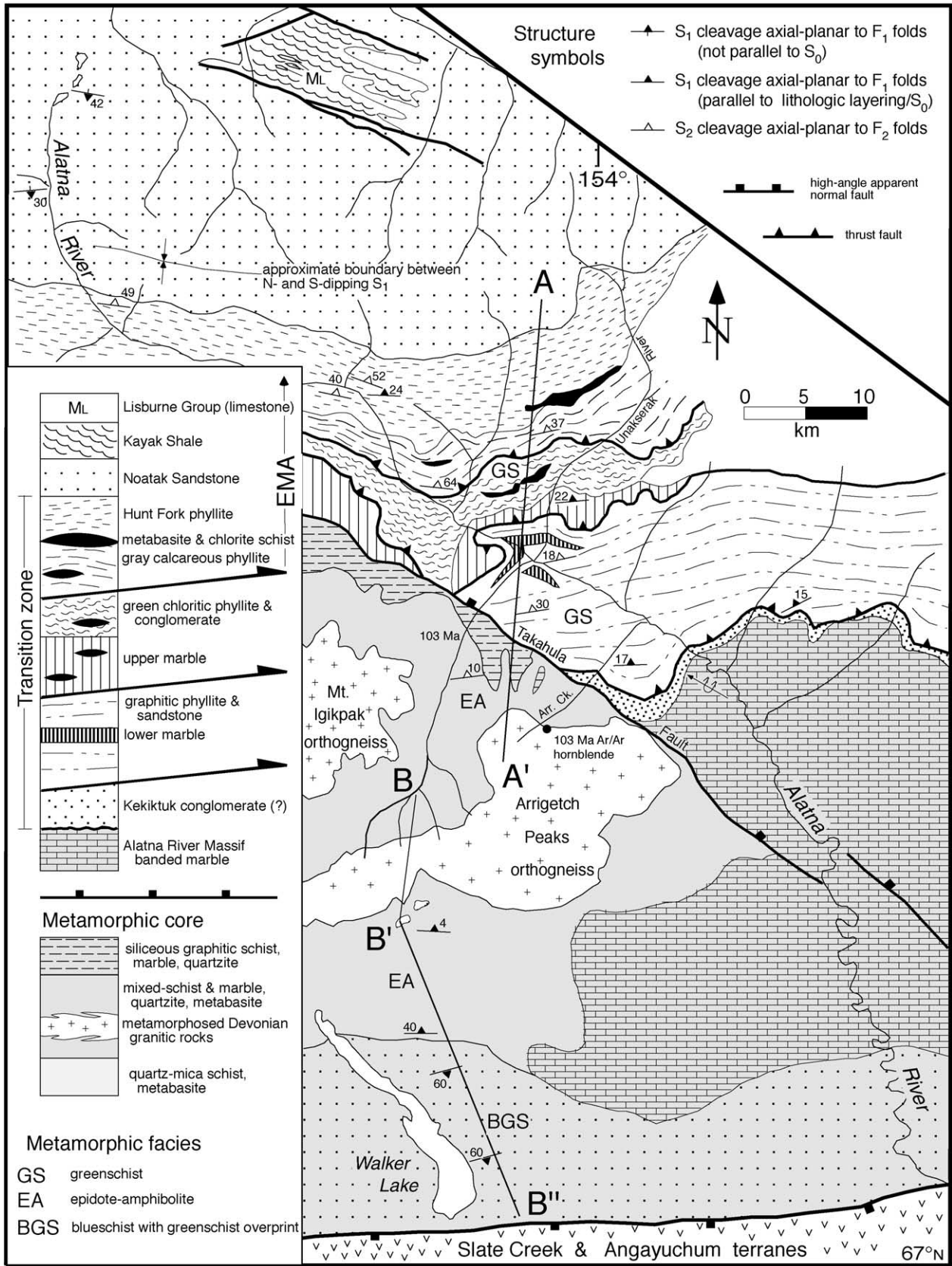


Fig. 2. Geologic map of study area and surrounding region. Geology near B¹–B² section from Patrick et al. (1994) and Dinklage (1998). Other geology from this study and Nelson and Grybeck (1980).

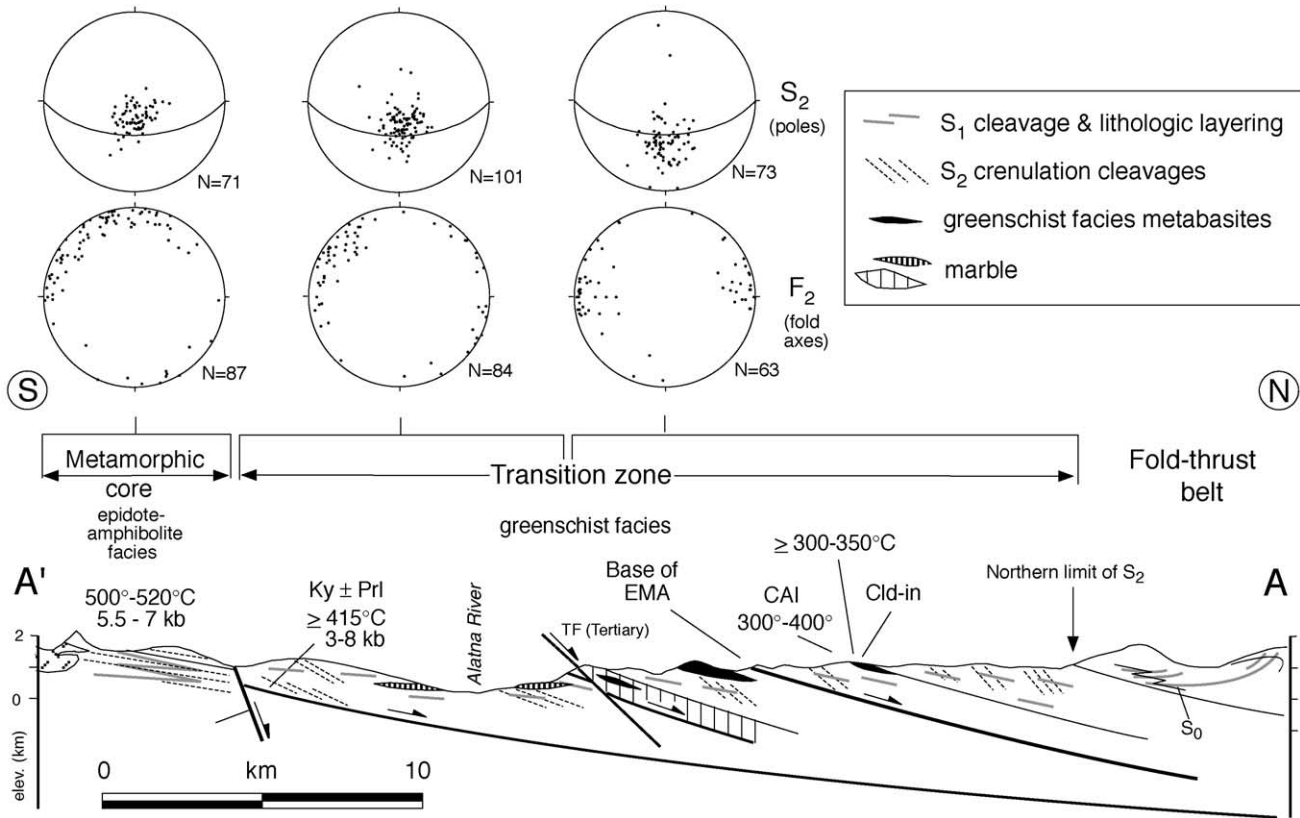


Fig. 3. Cross section A–A' and stereoplots of D_2 fabric data across detailed map area. See Fig. 2 for location. A 30° dipping plane is shown on stereoplots to highlight the southward decrease in S_2 dips. S_1 is generally parallel to shallowly N-dipping lithologic contacts and layering. Shallowly N-dipping faults are D_1 N-directed thrust faults that have subsequently been rotated. Note: contacts from map in Fig. 2 are shown, but not patterns. Also shown are peak metamorphic pressure–temperature constraints, chloritoid (Cld)-in isograd and temperature estimate from conodont alteration index (CAI, from Nelson and Grybeck, 1980). See Vogl (2000) for metamorphic data. Ky = kyanite; Prl = pyrophyllite; TF = Takahula Fault.

commun., 1996), which overlies a several-kilometer-thick section of much less competent phyllite and marble units (Fig. 2). Metabasites, thought to be sills and flows of Devonian age (Nelson and Grybeck, 1980), occur within phyllites and marbles in the middle part of this section (Figs. 2 and 3). The phyllite-dominated section overlies <100 m of quartzite and conglomerate, with minor lenses of schist, phyllite and marble lenses that may in part be structural slices of underlying units. I believe that the quartzite, conglomerate and some of the schist were correctly correlated with the Mississippian Kekiktuk conglomerate by Nelson and Grybeck (1980). The Kekiktuk conglomerate overlies a several-kilometer-thick sequence of banded marble that forms prominent peaks and ridges along the Alatna River to the southeast. No fossils have been reported within these marbles, which we refer to informally as the Alatna River massif in order to distinguish them from the thinner marble layers higher in the section.

The base of the Endicott Mountains allochthon is taken to be the base of the gray calcareous phyllite, although the original stratigraphic and paleogeographic position of the underlying phyllites and marbles is

unclear because of lack of precise fossil ages. Lithologically similar units (Hammond terrane) in the same structural position to the east, along the Dalton Highway, were inferred by Moore et al. (1997) to represent the stratigraphically deeper part of the Endicott Mountains allochthon. If the correlation of quartzite/conglomerate with the Kekiktuk conglomerate is correct, then the Kekiktuk, the Alatna River massif and possibly overlying graphitic phyllite (if Mississippian in age) would belong to the paraautochthonous North Slope subterrane of Moore et al. (1994). These correlations require further study, but are not critical to the results presented in this paper.

South of the Takahula Fault, a chloritoid-bearing, quartzose graphitic phyllite and quartzite unit with minor marble overlies a mixed-schist and marble unit along a gently NNW-dipping contact (Figs. 2 and 3). The mixed-schist and marble unit includes banded marble, calcic pelitic schist, calc-schist, quartzite and metabasite. These rocks were intruded by shallow level Devonian granitic plutons. The second largest of these plutons, the Arrigetch Peaks orthogneiss, crops out in the southern part of the study area (Figs. 2 and 3).

4. Deformation events

The structures and fabrics are discussed in terms of three deformational events: D_1 , D_2 and D_3 . D_1 includes the relatively well-documented dominant phase of N-directed deformation that led to the development of the fold–thrust belt. The D_1 structures are described and interpreted briefly, since the post- D_1 structural development is the main focus of this paper because of the controversy surrounding these events.

4.1. D_1 deformation

Reconnaissance traverses show that at the highest structural levels, represented by the competent Noatak Sandstone, D_1 produced kilometer-scale N-vergent asymmetric folds with E–W axes and a moderately S-dipping axial-planar solution cleavage (S_1) developed within fine-grained units (Fig. 3). Deeper parts of the Noatak Sandstone exposed farther south display tighter folds with more gently dipping axial planes. Handschy (1998) described similar features at correlative structural/stratigraphic levels near the Dalton Highway and inferred a progressive downward increase in shear strain approaching the base of the EMA; the sense of shear is consistent with northward displacement.

Strain increases downward near the Noatak/Hunt Fork contact, but the contact is demonstrably stratigraphic. Within the Hunt Fork and underlying phyllites, S_1 is a penetrative foliation defined by aligned metamorphic white mica and chlorite in phyllites, and by syn- D_1 actinolite and chlorite in metabasite lenses. Thus, D_1 deformation occurred at greenschist–facies conditions.

S_1 dips gently northward where it is unaffected by D_2 folding, and contains a locally well-developed, shallowly N-plunging lineation defined by mica streaking and long axes of strain shadows. The foliation is generally parallel to bedding except in fold hinges, where it is axial-planar to outcrop and smaller scale class 1c to class 2 isoclinal folds (Ramsay, 1967) with subhorizontal, W- to N-trending axes. At thin-section scale, S_1 is commonly a pervasive crenulation cleavage (S_{1b}), that is axial-planar to folds of an earlier bedding-parallel cleavage (S_{1a}), which is probably the result of early isoclinal folding. Complete transposition associated with centimeter-scale folding is observed in some thin-sections. Quartz is recrystallized and polygonal, displaying no grain-shape fabric. Because distinct marker beds are absent, the largest scale of F_1 folding within the individual phyllite units is not known. Any map-scale folds must be restricted to individual units since individual map units are not repeated in large-scale fold nappes.

The upper and lower marbles display a strong banding (pure marble) or flaggy cleavage (graphitic marble) and a well-developed N-trending stretching lineation. The banding dips gently northward and is commonly folded into meter- to centimeter-scale, asymmetric N-vergent folds with little or no axial-planar fabric development.

The marbles also display asymmetric strain shadows around crinoid stem fragments and locally well-developed oblique calcite grain-shape fabrics, both of which indicate top-to-the-north shear. Boudins of various scales, strain shadows around pyrite grains, and stretched cobbles and fossils indicate approximate plane strain with minimum $X:Z$ strain ratios of 8:1 locally within marbles and phyllites of the transition zone.

In the metamorphic core, south of the Takahula Fault, post- D_1 strain is higher than in the transition zone, and has severely overprinted D_1 structures. The preserved D_1 fabric in the metamorphic core is a white mica \pm chlorite foliation subparallel to lithologic layering, which has been folded about tight, recumbent F_2 folds. The S_1 foliation in the schists was commonly overgrown by chloritoid or garnet + biotite porphyroblasts. Thermobarometry indicates that garnet and biotite porphyroblasts grew during heating and reached peak temperatures of 500–520 °C at pressures of \sim 5.5–7 kb (Vogl, 2000). These data indicate that the D_1 foliation formed at upper greenschist–facies conditions and was subsequently overgrown by porphyroblastic mineral assemblages of lowermost epidote–amphibolite facies.

On the basis of the increase in intensity of S_1 fabric development and the decrease in S_1 dips toward the base of the EMA, the S_1 fabrics in the phyllites and marbles in the transition zone are interpreted to be the result of a broad zone of distributed N-directed shear associated with final emplacement of the EMA and underlying transition zone rocks, perhaps over the parautochthonous North Slope subterrane (if the transition zone overlies the Kekiktuk Conglomerate). High shear strains are suggested by the progressive decrease in dip of S_1 between the Noatak Sandstone, which is deformed by large-scale asymmetric folds with relatively little penetrative strain, and the underlying highly strained phyllites. The S_1 fabrics in the metamorphic core likely formed during the same N-directed shearing deformation event.

The north to south change in orientation of S_1 from south dips to north dips defines a synform with a hinge trace approximately located by my reconnaissance work near the southernmost exposures of the Noatak sandstone (Figs. 2 and 3). This synform probably resulted from the original downward decrease in dip of S_1 (presumably to horizontal or shallow south dips) toward the base of the Noatak Sandstone, combined with post- D_1 differential uplift/exhumation of the metamorphic rocks to the south, which rotated layering and N-directed thrust faults to north dips.

4.2. D_2 and D_3 deformation

As a result of differences in metamorphic grade and lithologic character, the structural style and amount of strain resulting from post- D_1 deformation varies between the transition zone and metamorphic core. Thus, post- D_1 structures in these two areas are described separately. D_2 and D_3

deformation are discussed together because in the metamorphic core the effects of each event are difficult to separate, as discussed below.

4.2.1. Transition zone—description

Although map-scale F_2 folds were not observed within the transition zone, outcrop-scale F_2 folds are widespread at all structural levels below the base of the Noatak Sandstone. F_2 folds range from gentle to close, with the tighter folds approaching similar geometries. F_2 folds display a consistent S-vergent asymmetry defined by both unequal limb length and axial surfaces that are not normal to the enveloping surface (Fig. 4a–d). Backlimbs of S-vergent folds are typically subhorizontal to gently dipping, while forelimbs range from moderately S-dipping to steeply N-dipping. F_2 fold axes are subhorizontal and trend \sim E–W, but commonly have trends more to the NW in the deeper parts of the section to the south (Fig. 3). Axial-planar S_2 cleavages dip northward between 20 and 60° (Fig. 3), and dip more steeply than the regional dip of the units and S_1 layering. Locally, within alternating quartzite/phyllite units, S-vergent F_2 folds with axial-planar S_2 are detached from underlying relatively planar quartzite and conglomerate (Fig. 4e), which displays a top-to-the-south quartz grain-shape fabric (Fig. 4f), but only very weak discontinuous S_2 .

The upper and lower marble units are typically not folded with the adjacent phyllites, and they only locally display weak S_2 cleavages. In general, the upper and lower marbles appear to preserve small-scale strain features (discussed above) that formed during D_1 . In contrast, marbles along the Kekiktuk/Alatna River massif contact commonly display mesoscopic S-vergent F_2 folds (Fig. 4d and g), which are locally detached from underlying planar banded marbles (Fig. 4g). These marbles also contain an S_2 solution cleavage that dips moderately northward, more steeply than the marble banding.

Repetition of units by map-scale D_2 thrust faults was not observed, and the lack of marker units and discontinuous outcrop made it difficult to identify faults within individual map units. At least two apparent outcrop-scale S-directed thrust faults were observed, however, in the Unakserak River region. One of these faults duplicates the lower marble along a shallowly N-dipping fault, and is associated with a N-dipping S_2 crenulation cleavage that dips more steeply than the fault. The second example occurs within quartzose phyllites farther north, where a 20° N-dipping fault, parallel to relatively planar S_1 in the hanging wall, truncates subhorizontal layering in the footwall. The hanging wall contains decimeter-scale S-vergent kinks.

Shallowly to moderately N-dipping, N-side-down normal faults with displacements up to \sim 100 m were observed in the Unakserak River valley region (Fig. 5), and are assigned to the D_3 deformation event. Other D_3 -related structures include shallowly to moderately N-dipping brittle/ductile shear bands with N-side-down offsets that locally cut relatively competent units. Although similar in orientation and

geometry to S_2 cleavages, the shear bands differ by showing discrete offsets as opposed to apparent offsets produced by dissolution.

Clastic rocks of the transition zone preserve two to three cleavage generations. Widespread N-dipping S_2 crenulation cleavages cut subhorizontal S_{1a} and subhorizontal to S-dipping S_{1b} . S_2 cleavages range from discrete to zonal, and contain greater amounts of insoluble residues and lesser amounts of quartz relative to microlithons, indicating significant dissolution. This dissolution has created alternating zones of chlorite- and white mica-rich domains (M-domains) and quartz-rich domains (Q-domains) (Fig. 6a–d). Although phyllosilicates occur along S_2 planes, they appear to be rotated syn- D_1 grains.

Kyanite occurs locally within aluminous quartzites and quartzose schists of the Kekiktuk Conglomerate. Kyanite preserves straight inclusion trails of S_1 , whereas the matrix foliation is locally tightly folded, indicating that the deepest levels of the transition zone were heated to peak temperatures of $> \sim 415$ °C (pyrophyllite breakdown) following D_1 . Albite and chloritoid also occur locally within the deepest units of the transition zone and generally preserve similar straight inclusion S_1 trails. Locally, however, inclusion trails in small (< 1 mm across) albite porphyroblasts are straight within the cores, but display curvature near the rims (Fig. 6c). The curvature has the same sense as that of S_1 rotated into S_2 planes outside the porphyroblast margins (Fig. 6c). These relations are interpreted to indicate that the early stages of S_2 locally overlapped with porphyroblast growth.

N-dipping S_2 cleavages are locally axial-planar to S-vergent F_2 folds, but in many outcrops S_2 cannot be clearly related to folds of a scale larger than the crenulations. Where S_1 is subhorizontal to gently S-dipping, S_2 crenulation cleavages are commonly asymmetric due to preferential dissolution on the north limbs of antiformal crenulation folds (Fig. 6a–d). Where S_2 cleavages are discrete, or M-domains are narrow compared with Q-domains, S_1 layering across the S_2 cleavages shows N-side-down deflections and ‘normal-sense’ apparent offsets (Figs. 4c and 6a–c), which superficially resemble extensional crenulation cleavages (Platt and Vissers, 1980) or shear bands (Hanmer and Passchier, 1991). There is a complete gradation, however, commonly within a single thin section, between thin discrete seams of S_2 (Fig. 6a and b-bottom) and zonal S_2 , where the width of M-domains is several times that of the Q-domains (Fig. 6a–d). Where the M-domain/Q-domain width ratio increases, the crenulations take on a S-vergent asymmetry (Fig. 6a, b and d). Identical crenulation cleavage relationships can be found from the micro-scale to the decimeter-scale (compare Fig. 6b and e). These relationships are found on both the long backlimbs of S-vergent F_2 folds (Fig. 4c) and in outcrops not displaying mesoscopic folds; geometric relationships are identical in both cases.

Where S_1 enveloping surfaces approach moderate to steep

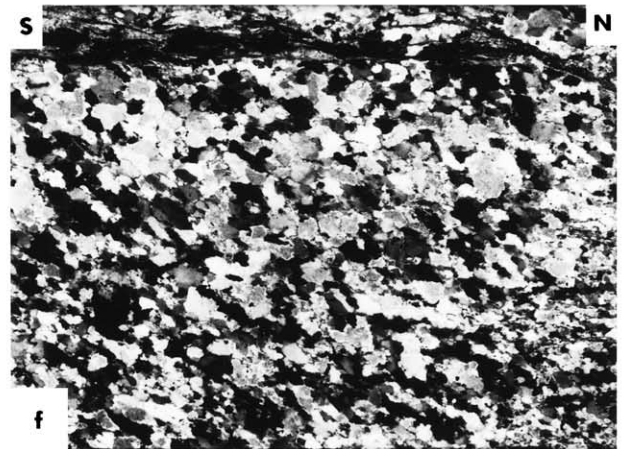
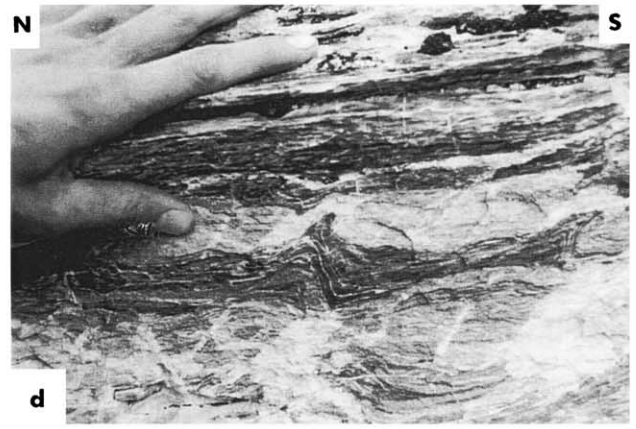
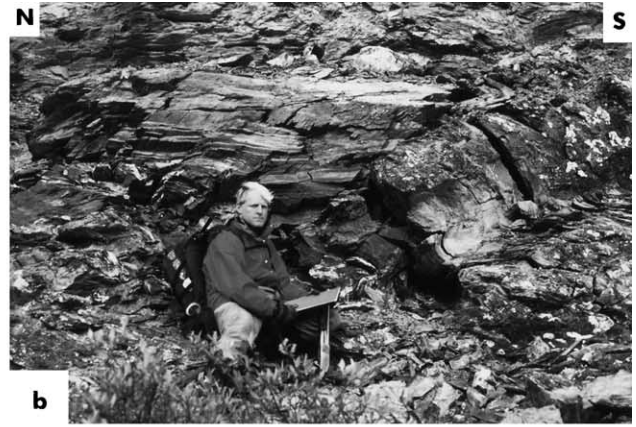




Fig. 5. North-dipping D_3 normal fault in the transition zone. Fault places banded gray marble (left) against phyllite and sandstone (right).

south dips, such as on the forelimbs of F_2 folds, discrete S_2 cleavages often show top-to-the-south deflections and ‘reverse-sense’ apparent offsets across S_2 (Fig. 6d), as well as more symmetric crenulations. These relationships are also scale independent.

In contrast to recrystallized D_1 strain shadows, D_2 strain shadows around pyrite locally preserve quartz fibers. Displacement-controlled fibers, shapes of face-controlled fiber pressure shadows, and elongate quartz grains in millimeter- to centimeter-scale folded quartz veinlets are parallel to S_2 , indicating that S_2 parallels the plane of flattening. Three-dimensional pressure shadow shapes suggest approximately plane strain. Pressure shadows and folded veins indicate D_2 $X:Z$ strain ratios between 1.5:1 and 2.5:1, but strains may be greater where crenulations are tighter in the southernmost part of the transition zone.

4.2.2. Transition zone—interpretation

The descriptions above indicate that D_2 structures in the transition zone formed during a top-to-the-south deformation. One of the diagnostic features is the presence of consistently S-vergent folds. Fold vergence, however, is not always a reliable shear-sense indicator because it is a function of the original angle between the maximum shortening direction and layering, and also because fold vergence may reverse during progressively higher shear strains (e.g. Ramsay et al., 1983; Krabbendam and Leslie, 1996). The folds described here are considered to record S-directed deformation because: (1) they are locally detached from

underlying planar layering exhibiting top-to-the-south quartz grain-shape fabrics, (2) they display a N-dipping axial-planar cleavage, (3) they are associated with low strains, and (4) folds with sheared-over hinges, such as in Fig. 4d, clearly require top-to-the-south shearing. The presence of small-scale S-directed thrust faults also indicates S-directed deformation.

The widespread development of asymmetric S_2 cleavages with N-side-down deflections and apparent offsets in the transition zone is the result of the initial angle between the N-dipping D_2 flattening plane and the original orientation of S_1 layering (i.e. S_1 dips less steeply northward than the D_2 flattening plane). The dominance of this cleavage geometry over those with apparent top-to-the-south offsets is likely due to the regional-scale gently dipping S_1 layering and the greater chance of exposing long backlimbs relative to short forelimbs of S-vergent folds.

The presence in the transition zone of N-side-down normal faults and brittle/ductile N-side-down shear bands with discrete offsets indicates that the area was also affected by N–S horizontal extension, which is referred to as D_3 . This extension may have reactivated S_2 cleavages with minor normal-sense slip, as suggested by the presence of solution surfaces in small-displacement normal fault zones.

4.2.3. Metamorphic core—description

In the epidote–amphibolite grade rocks south of the Takahula Fault, post- D_1 deformation is characterized by kilometer-scale tight- to isoclinal recumbent folds with axial planes that dip $\sim 10^\circ$ north or northwest (Fig. 7). These F_2 folds, defined by marble bands up to ~ 60 m thick, display no obvious vergence. Vergence of folds parasitic to mesoscopic folds reverses across the axial planes. Fold-axis orientation of the map-scale folds was difficult to establish, but mesoscopic F_2 folds plunge gently between west and north (Fig. 3). Many more N–S-trending folds were observed in lithologies where it was difficult to distinguish between F_1 and F_2 folds; these were not included in the stereoplots of Fig. 3. The F_2 folds in the metamorphic core show substantial thickening in the hinge, and approach similar geometries.

F_2 folds have a gently N-dipping axial-planar crenulation cleavage (S_2) that is well-developed in mica-rich layers. Depending on lithology, the dominant foliation in outcrop varies between S_1 layering rotated during F_2 folding and S_2 crenulation cleavages that have completely overprinted S_1 .

Fig. 4. South-directed D_2 mesoscopic structures in transition zone. (a)–(c) S-vergent folds in quartzose phyllites and metapsammite. Note N-side-down ‘normal’-sense deflections and apparent offsets on long backlimb to the right giving shear-band appearance in (c). (d) S-vergent folds with sheared-over hinges (middle dark band) in banded marble at the base of the transition zone. (e) S-vergent folds in dark quartzite (thin band below hammer) with intervening quartz–mica schist (light color) displaying shallow N-dipping S_2 crenulation cleavage. These units lie above relatively planar quartz–cobble conglomerate (immediately below photo) that displays top-to-the-south quartz grain-shape fabrics shown in (f). (f) Photomicrograph of quartz matrix in conglomerate below detached S-vergent folds in (e). Shows top-to-the-south quartz grain-shape fabrics. Photo is ~ 3.2 mm across. (g) S-vergent folds of contact between orange (OM) and gray marble (GM). Shows N-dipping axial-planar S_2 crenulation cleavage. Folds and cleavages do not affect underlying relatively planar marble at the level of the hammer head. All fold axes trend \sim E–W in these photos. Hammer is ~ 39 cm long.

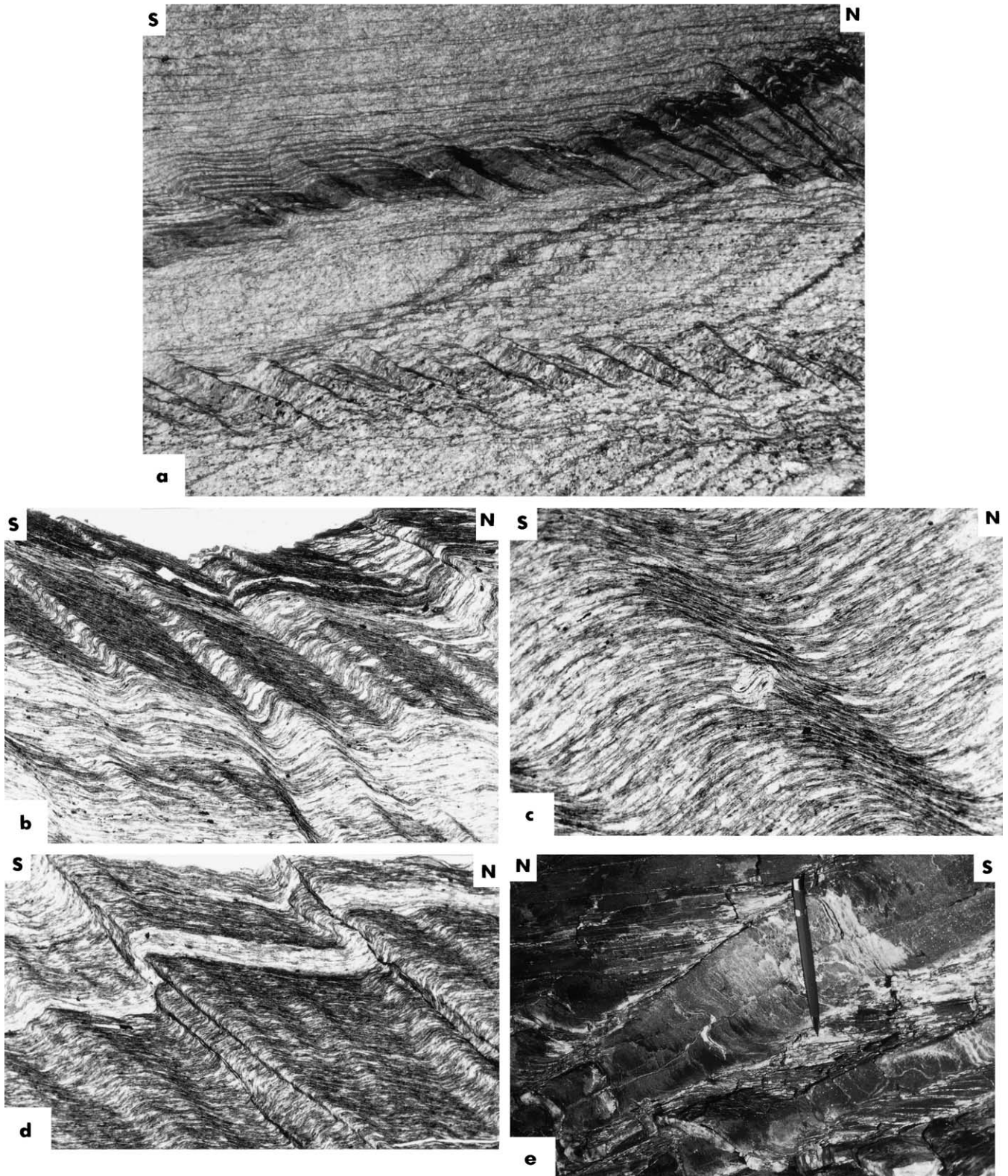


Fig. 6. D₂ Microstructures from transition zone. (a) Shallowly N-dipping discrete cleavages overprinting S_{1a} (predominantly S-dipping in photo) and S_{1b} (horizontal). Lower band of discontinuous S₂ has consistent N-side-down, normal-sense apparent offsets; similarly oriented S₂ in upper band has variable geometries, including asymmetric S-vergent folds (left edge). Photo is ~6.5 mm across. (b) N-dipping S₂ cleavages. Note consistent differentiation on north limb of antiformal crenulations. Where the ratio of microlithon width to S₂ width increases, the geometry changes from asymmetric S-vergent folds (upper half of photo) to 'normal'-sense apparent offset (lower part of photo). Photo is ~3.2 mm across. (c) N-dipping S₂ cleavage partially containing albite porphyroblast. Graphitic inclusion trails in albite curve into S₂ near the porphyroblast margins. Photo is ~1.3 mm across. (d) S-vergent microfolds with discrete N-dipping axial-planar cleavage on forelimb. Note apparent top-to-south offsets across S₂ and differentiation on long limbs. From same thin-section as (b), but where S₁ enveloping surface dips south. Photo is ~3.2 mm across. (e) Macroscopic differentiated crenulation cleavages. Subhorizontal S₁ regions are differentiated phyllosilicate-rich domains. Moderately to steeply dipping S₁ are quartz-rich domains. Note similarity to (b). Pencil for scale.



Fig. 7. Kilometer-scale M-shaped fold defined by resistant marble bands in metamorphic core. Ridge trends ~N–S and stands ~700 m above valley bottom.

N–S stretching lineations, defined by mica streaking, elongate quartz grains and strain shadows around porphyroblasts, are well-developed on both S_2 cleavage surfaces (L_2) and on the S_1 foliation (L_1), where they have been folded around F_2 fold hinges.

The S_2 crenulation cleavages range from discrete to zonal, with many samples showing both types. Discrete cleavages vary from thin pressure solution seams to white mica-rich (with minor chlorite) bands that truncate microfolds of S_1 . Crenulation folds vary in tightness and range from symmetric to asymmetric, with the sense of asymmetry related to the position relative to hinges of mesoscopic folds.

Quartzose schists within the epidote–amphibolite facies rocks contain biotite \pm garnet or chloritoid porphyroblasts that preserve inclusion trails (S_i) of quartz, ilmenite, epidote or graphite. Most commonly, S_i is either straight, or curves only near the porphyroblast margins (Fig. 8). Less commonly, S_i curves more continuously between the core and rim. S_i curvatures are generally $<90^\circ$, but are locally higher. Where S_2 is not developed or is widely spaced, S_i is generally continuous with, but rotated with respect to matrix S_1 (Fig. 8a–e). Where S_2 is more pervasively developed, S_i is discontinuous with S_2 and typically oriented at a high angle to S_2 , which commonly wraps around porphyroblast margins (Fig. 8f). Pressure shadows are generally well developed around porphyroblasts, and are commonly symmetric; more asymmetric examples give ambiguous shear senses.

The sense of rotation of curved S_i varies throughout the area, as does the relative sense of porphyroblast– S_1 rotation shown by straight S_i that is continuous with, but oblique to, S_1 (Fig. 8). Where samples can be located with respect to position around mesoscopic F_2 folds, the relative sense of S_i curvature and porphyroblast– S_1 rotation reverses across the axial plane and is consistent with the vergence of parasitic folds (Fig. 8g). From this relationship (and from the abun-

dance of straight inclusion trails), it is inferred that the S_i curvature preserved inside some porphyroblast margins records the incipient stages of F_2 folding rather than continued D_1 deformation. Thus, it is concluded that D_1 asymmetry is not preserved in the porphyroblasts, and that mesoscopic and smaller-scale shear-sense indicators may locally be related to early stages of folding and not be representative of the bulk kinematics of the strain in the metamorphic pile. Assuming the porphyroblasts have rotated with respect to F_2 axial planes, this opposing sense of porphyroblast–matrix rotation may be due to flexural flow/slip folding.

Overall, the combination of porphyroblast–matrix relationships and thermobarometry (Vogl, 2000) indicate that D_2 crenulations associated with initial stages of F_2 folding commonly initiated during growth of porphyroblast rims during a temperature increase to near 520°C (at ~ 5.5 – 7 kb; Vogl, 2000). Pressure changes during porphyroblast growth have been difficult to ascertain (Vogl, 2000), but are being further investigated. Much of the D_2 strain and S_2 cleavage development accumulated during tightening of the folds following porphyroblast growth. Although retrogression of metamorphic minerals, including local complete replacement of garnet by chlorite, was observed, retrogression occurred after S_2 development. Thus, temperatures may have remained near the peak during formation of S_2 .

Quartz within the metamorphic core is fully recrystallized and polygonal. Calcite grains are slightly elongate in some marbles and define a N-trending lineation and weak foliation parallel to the axial-planar S_2 in the adjacent schists. To assess whether a lattice-preferred orientation within the quartzites of the metamorphic core might delineate a strongly non-coaxial shear zone, quartz c -axis orientation was measured in three quartzites. Two samples were collected from the contact between the graphitic quartzose fine-grained schist and the underlying mixed-schist and marble unit to evaluate whether this contact might be a zone of concentrated non-coaxial deformation. These samples, as well as a third sample from slightly deeper in the section, show two intersecting girdles (Fig. 9) that imply an absence of simple shear strain that has dominated the crystallographic orientation distribution.

Despite large Mesozoic strains, the north margin of the Devonian Arrigetch Peaks orthogneiss locally preserves intrusive relationships as evident in the presence of indurated calc–silicate contact skarns and other emplacement-related mineralized zones. Although metamorphosed, much of the granitic orthogneiss is weakly strained. Locally, however, the granitic rocks are strongly foliated and lineated, with the most pervasive fabrics developed near the contacts with interfingering metasedimentary rocks. Spaced brittle–ductile shear surfaces occur in some areas and display elliptical mica aggregates defining a N–S lineation. The shear surfaces and other foliations are commonly folded, along with S_1 layering in the metasedimentary rocks, into orientations that suggest that the fabrics at the margins

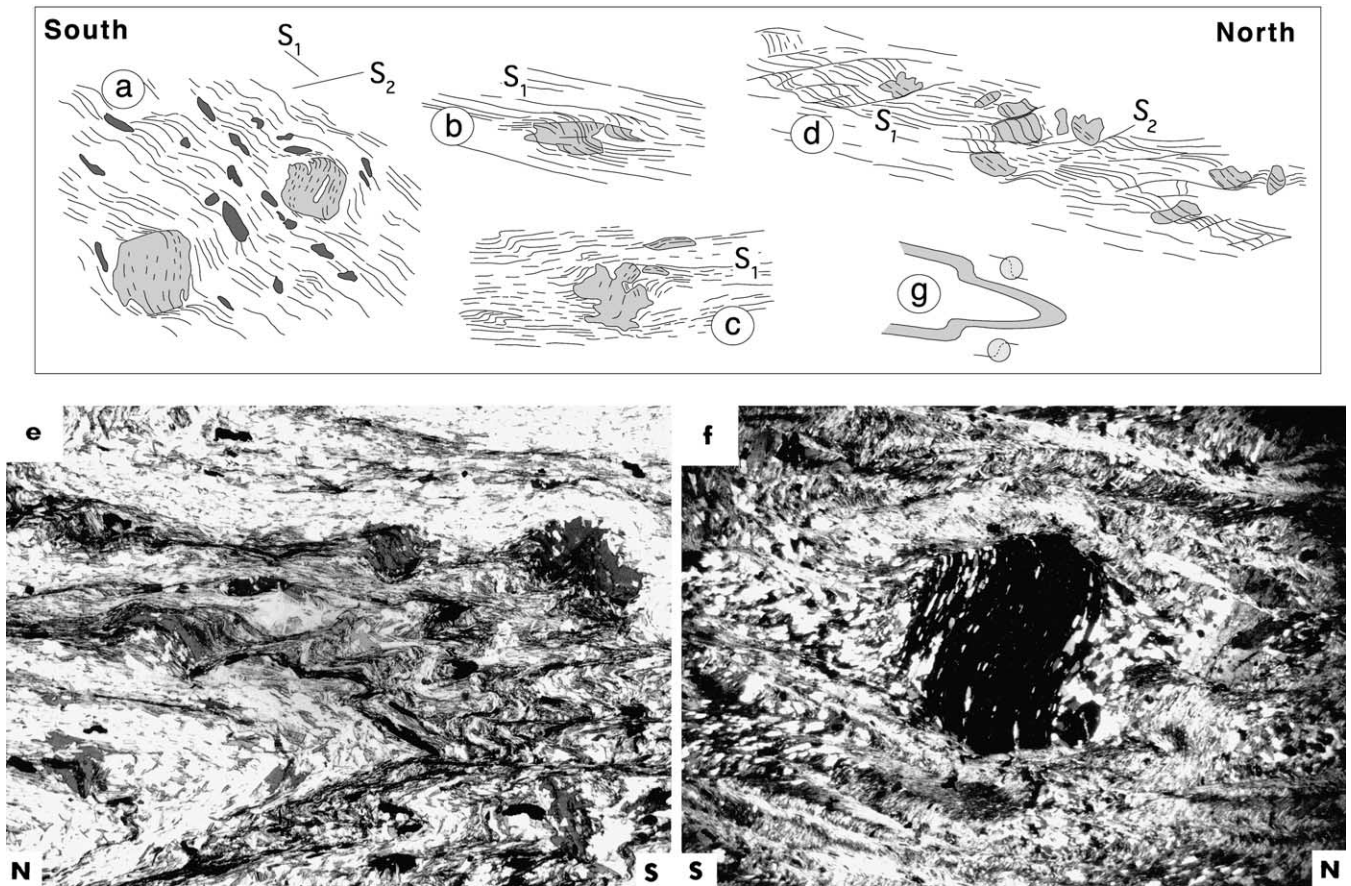


Fig. 8. Line tracings and photomicrographs of porphyroblast-matrix relationships within epidote-amphibolite grade quartzose schists of the metamorphic core. (a) Garnet porphyroblasts (light gray) from the lower limb/hinge region of a mesoscopic S-closing F_2 fold. Shows incipient axial-planar S_2 development along with slight rotation of garnets with respect to S_1 . (b) Chloritoid porphyroblast that grew during top-to-the-north rotation of porphyroblast relative to S_1 layering. (c) Biotite porphyroblast that grew during top-to-the-south rotation of porphyroblast relative to S_1 layering. (d) Biotite porphyroblasts which grew pre- to syn-kinematically during top-to-the-north rotation of porphyroblast relative to S_1 layering. Shows S_2 which is axial-planar to tight mesoscopic SW-closing F_2 fold. Sample is from lower limb. (e) Centimeter-scale F_2 folds and syn- to post-kinematic biotite porphyroblasts. Note biotite in upper middle part of photo with top-to-the-south rotation sense with respect to S_1 . Photo is ~ 6.2 mm across. (f) Strongly developed S_2 crenulation cleavage that post-dates growth of garnet porphyroblast. Along upper margin of garnet, quartz inclusion trails curve into folded S_1 , suggesting initial crenulation occurred during growth of porphyroblast margin. Photo is ~ 13 mm across. (g) Schematic sketch showing consistency between fold vergence and relative porphyroblast-matrix rotation on fold limbs. All sections are perpendicular to foliation and parallel to N-trending lineation.

of the orthogneiss formed during D_1 and were folded during D_2 .

Slightly asymmetric foliation boudinage with a top-to-the-north shear sense is common within homogeneous quartzose schists (Fig. 10). Moderately N-dipping ductile shear bands occur in schistose rocks, while brittle-ductile shear bands are found cutting metabasites; shear bands consistently show N-side-down offsets. These structures, which indicate a component of subhorizontal extension, must have formed after much of the strain accumulated and are assigned to D_3 .

4.2.4. Metamorphic core—interpretation

It is proposed that the post- D_1 kinematic development in the metamorphic core is the result of the same sequence of D_2 backfolding and D_3 extension delineated in the transition zone. In the metamorphic core, however, the distinction between structures formed during D_2 and D_3 is not straight-

forward, and therefore this interpretation requires discussion. The inferred two-stage (D_2 and D_3) development of structures formed in the metamorphic core and transition zone is shown schematically in Fig. 11.

Porphyroblast-matrix relationships suggest that the early crenulation stage of F_2 folding is recorded by curvature of inclusion trails inside the porphyroblast margins. Although less common than in the metamorphic core, porphyroblasts in the transition zone have similarly shaped inclusion trails and relationships with cleavages. In the transition zone the S_2 cleavages are clearly associated with S-vergent F_2 folds. Thus, it is inferred that folds in the metamorphic core also initiated from S-directed deformation (Fig. 11). Although it is tempting to interpret all of the post- D_1 strain in the metamorphic core as a higher-strain, deeper level manifestation of the S-vergent deformation in the transition zone, the lack of kinematic indicators suggesting large amounts of top-to-the-south shear strain preclude such an

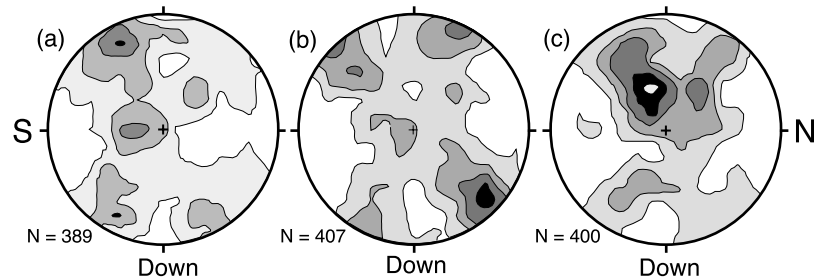


Fig. 9. Quartz *c*-axis fabrics from quartzites of metamorphic core. All lower-hemisphere, equal-area projections viewed towards the west. Only foliation (S_1) dips gently northward.

interpretation. Instead, it is suggested that a significant amount of the post- D_1 strain accumulated during D_3 N–S horizontal extension and vertical thinning (Fig. 11). Since normal faults such as those found in the overlying transition zone are not present in the metamorphic core, extension was likely accommodated by other more ductile processes, such as S_2 axial-planar cleavage development associated with tightening of earlier formed F_2 folds (Fig. 11). After a strong anisotropy formed following the more advanced stages of cleavage development and tightening of folds, extension was accommodated by layer-parallel extension, which formed the foliation boudinage and N-side-down shear bands. These features suggest a top-to-the-north shear component that may be the result of vertical thinning superimposed N-dipping layering.

The downward-shallowing of foliations formed during D_1 suggests that layering was subhorizontal following D_1 and there is no evidence for steepening of layering other than that related to D_2 backfolding. Furthermore, restoration of the layering to its pre- D_2 orientation using thermochronologic and metamorphic data also suggests that the layering was close to horizontal prior to D_2 folding. Thus, since layering would not have been in the shortening field for a horizontal extension, it is considered improbable that the F_2

folds in the metamorphic core were initiated and formed entirely during the extensional event.

In summary, the post- D_1 structures in the metamorphic core are not adequately accounted for by a single backfolding or extensional event. Instead a two stage deformational sequence involving F_2 folds initiating during S-vergent folding and tightening significantly during N–S horizontal extension is the simplest way to explain the structures in the metamorphic core, and is also most consistent with the deformational sequence more clearly preserved in overlying rocks.

5. Age of deformation

$^{40}\text{Ar}/^{39}\text{Ar}$ mica ages from the transition zone range from ~ 115 to ~ 97 Ma (Toro, 1998; Vogl et al., 2002). Vogl et al. (2002) suggest that the data sets define a bimodal distribution of ages, with an older set of ~ 112 – 115 Ma and a younger set around 97 Ma. On the basis of the relatively low (greenschist facies) temperatures of D_1 deformation, Toro (1998) and Vogl et al. (2002) suggest that the older ages of 112–115 Ma represent the age of mica growth during the last stages of D_1 . Vogl et al. (2002) interpret the younger ages (which can be found in the same outcrop as older ages) as the result of local, nearly complete resetting of the argon system during post- D_1 heating, which also led to porphyroblast growth in the metamorphic core and deeper levels of the transition zone.

We have obtained a plateau age of ~ 103 Ma from a hornblende sample from the north margin of the granitic orthogneiss in the metamorphic core (Fig. 2). Since peak temperature estimates of 500 – 520 °C (garnet–biotite thermometry; Vogl, 2000) from schists of the metamorphic core are similar to the estimated closure temperature for argon in hornblende, the 103 Ma hornblende age likely represents initial cooling from the metamorphic peak, and therefore provides a minimum age (but only a slight underestimate) for the peak of metamorphism. Porphyroblast–matrix relationships described above for the metamorphic core and deep parts of the transition zone suggest that D_2



Fig. 10. Foliation boudinage in homogeneous quartz-mica schists. Boudins are slightly asymmetric, suggesting a top-to-the-north shear component.

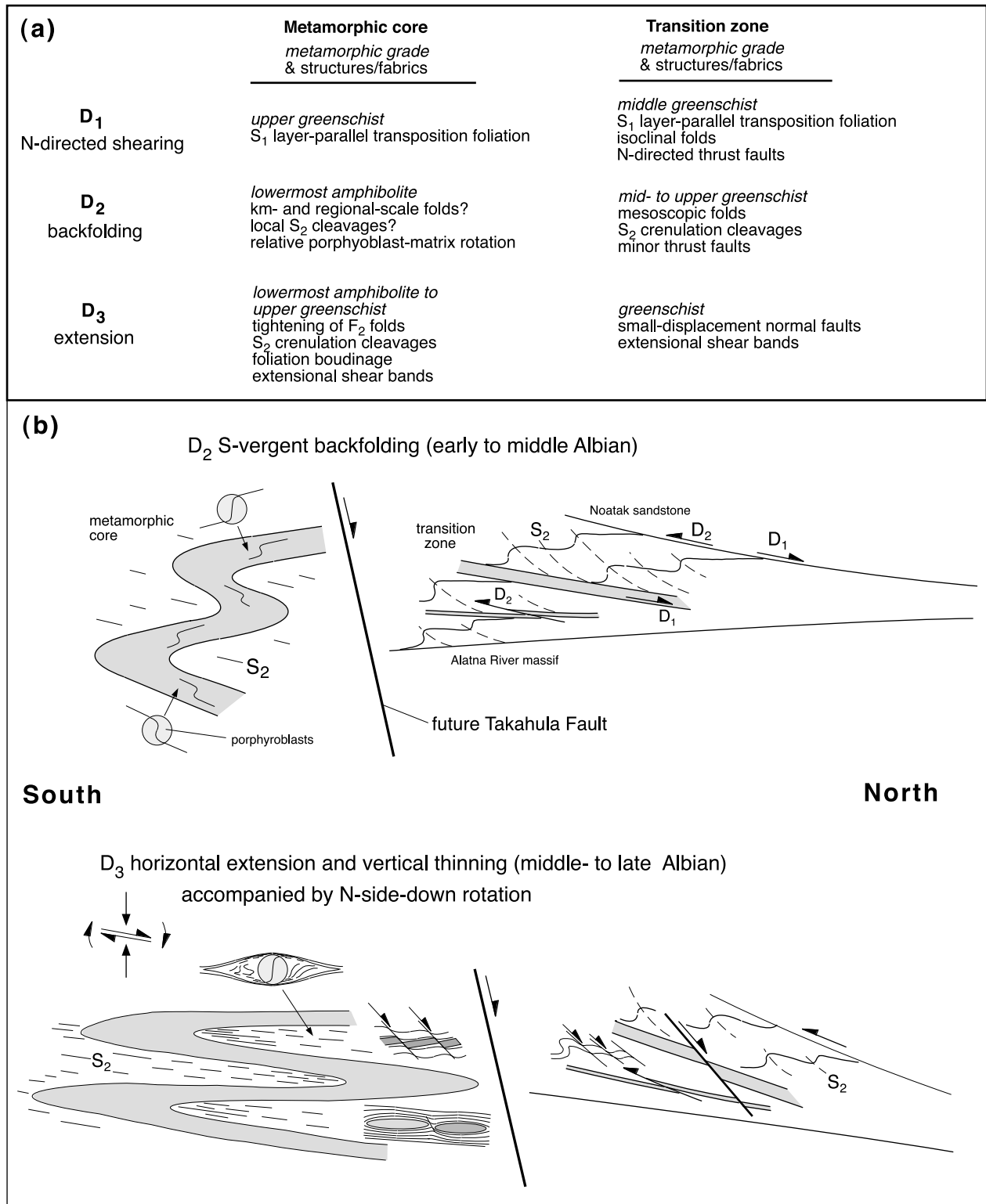


Fig. 11. Summary of structural development of the study area. (a) Summary of metamorphic grade and structures formed during three deformational events. (b) Schematic two-stage (D₂ and D₃) model to explain the distribution of post-D₁ folds and cleavages.

backfolding overlapped with the peak of metamorphism. Thus, we infer that S-vergent backfolding took place in the early- to mid-Albian.

Although most of the inferred D₃ extensional strain in the

metamorphic core occurred after porphyroblast growth, there is little evidence for significant retrogression during the crenulation cleavage development, suggesting elevated temperatures during D₃. Thus, the penetrative vertical

thinning associated with D_3 in the metamorphic core probably occurred during initial cooling from peak conditions, and therefore may be approximately dated by the ~ 103 Ma $^{40}\text{Ar}/^{39}\text{Ar}$ hornblende age. Hornblende and mica $^{40}\text{Ar}/^{39}\text{Ar}$ data delineate a short-lived period of relatively rapid cooling beginning at ~ 103 Ma and locally lasting only a few million years (Vogl et al., 2002). This cooling appears to be related to a widespread exhumation, which Vogl et al. (2002) attribute to a combination of extension and erosion. Furthermore, Vogl et al. (2002) document a southward increase in cooling and exhumation rates that is probably related to normal faulting on the south flank of the range during the ~ 103 Ma event. Thus, we infer that penetrative vertical thinning in the study area occurred at, and shortly after, ~ 103 Ma, and was synchronous with large-scale normal faulting on the south flank of the Brooks Range. A similar age for extensional shearing along these normal faults was suggested by Christiansen and Snee (1994).

D_3 extension and exhumation was accompanied by N-side-down rotation of layering in the study area. Rotation is demonstrated by the fact that metamorphic rocks near the southern margin of the Arrigetch Peaks orthogneiss (Fig. 2) were hotter and deeper than those in the study area (Vogl, 2000), but have similar $^{40}\text{Ar}/^{39}\text{Ar}$ hornblende cooling ages (of ~ 103 – 104 Ma; Vogl et al., 2002) and older mica ages (~ 96 Ma vs. 91–85 Ma).

6. Synthesis

Based on a combination of structural and thermochronologic data the following sequence of events for the structural section on the north flank of the metamorphic culmination is suggested. A protracted event of N-directed thrusting culminated around 112–115 Ma with final emplacement of the Endicott Mountains allochthon above a parautochthonous (?) sequence. N-directed D_1 thrusting resulted in a broad zone of distributed shear (transition zone) that spans the boundary between the EMA and the parautochthon. This strain produced subhorizontal greenschist-grade foliations, which overprint the inferred thrust boundary at the base of the EMA. Uppermost greenschist-grade S_1 foliations in the metamorphic core are probably also related to the same thrusting event. D_1 may be dated in the transition zone by $^{40}\text{Ar}/^{39}\text{Ar}$ ages of 112–115 Ma from synkinematic D_1 micas (Toro, 1998; Vogl et al., 2002), providing a minimum age for the emplacement of the EMA. Thermal re-equilibration reaching lowermost amphibolite facies conditions following D_1 resulted in post- S_1 porphyroblast growth and local resetting of argon ages in the deeper levels of the study area.

D_2 S-vergent backfolding followed the D_1 event, and produced widespread N-dipping crenulation cleavages and mesoscopic asymmetric S-vergent folds in the transition zone. In the metamorphic core, D_2 led to the initiation of crenulations and larger scale folds within epidote–amphi-

bolite facies rocks (Fig. 10). The S-vergent folding and crenulation-forming event occurred near the peak temperature as evident in S_1 curvature within porphyroblast margins. The sense of relative porphyroblast–matrix rotation reverses across the axial planes, indicating a folding event rather than a homogeneous shearing. An $^{40}\text{Ar}/^{39}\text{Ar}$ hornblende age of ~ 103 Ma probably slightly post-dates the peak of metamorphism, suggesting that D_2 backfolding occurred in the early- to mid-Albian.

Subsequent horizontal extension (D_3) produced small-displacement N-side-down normal faults in the greenschist-grade rocks. In the epidote–amphibolite grade rocks, D_3 extension produced, and enhanced an S_2 crenulation cleavage associated with tightening of F_2 folds. Increasing strain and N-side-down rotation during D_3 produced a strong N-dipping layering. Superimposition of extension on this layering led to the development of late-stage structures with a local top-to-the-N shear sense (Fig. 11). D_3 extensional strain has severely overprinted older structures and blurred the distinction between D_2 and D_3 structures in the metamorphic core. D_3 extension probably occurred during initial relatively rapid cooling from peak temperatures over a period of a few million years beginning around 103 Ma.

The only other study of a stratigraphically and metamorphically similar section in the Brooks Range was done by Toro (1998) in an area ~ 25 – 30 km to the west and along-strike of the study area. Toro (1998) suggested that top-to-the-N extensional shearing occurred along a N-dipping section following N-directed contractional D_1 . The model presented here is broadly similar to Toro's except for the recognition of S-vergent deformation, which is interpreted to have followed N-directed contractional deformation and pre-dated extension. My reconnaissance traverses along the northern Alatna River (Fig. 2) included the region directly north of Toro's transect, and revealed abundant S-vergent folds and N-dipping S_2 crenulation cleavages. S_2 represents the flattening plane and dips moderately northward, more steeply than layering, which is inconsistent with S_2 having formed during top-to-the-N extensional shearing along layering. These structures are not accounted for in Toro's analysis. Furthermore, as stated above, since evidence suggests that layering was subhorizontal following D_1 , it seems unlikely that F_2 folds in the metamorphic core initiated during horizontal extension. Thus, in contrast to Toro who interprets all post- D_1 cleavages and folds to extension, I assign most of the S_2 cleavage development in the greenschist-grade rocks to D_2 backfolding. Curved inclusion trails inside porphyroblast margins in epidote–amphibolite facies rocks to are also assigned to D_2 backfolding on the basis of correlation of similar inclusion trails in lower-grade rocks. In contrast, Toro assigned the inclusion trails to N-directed D_1 deformation. In both models, however, much of the S_2 crenulation cleavage development in the epidote–amphibolite facies rocks is attributed to D_3 (D_2 of Toro et al.) extension.

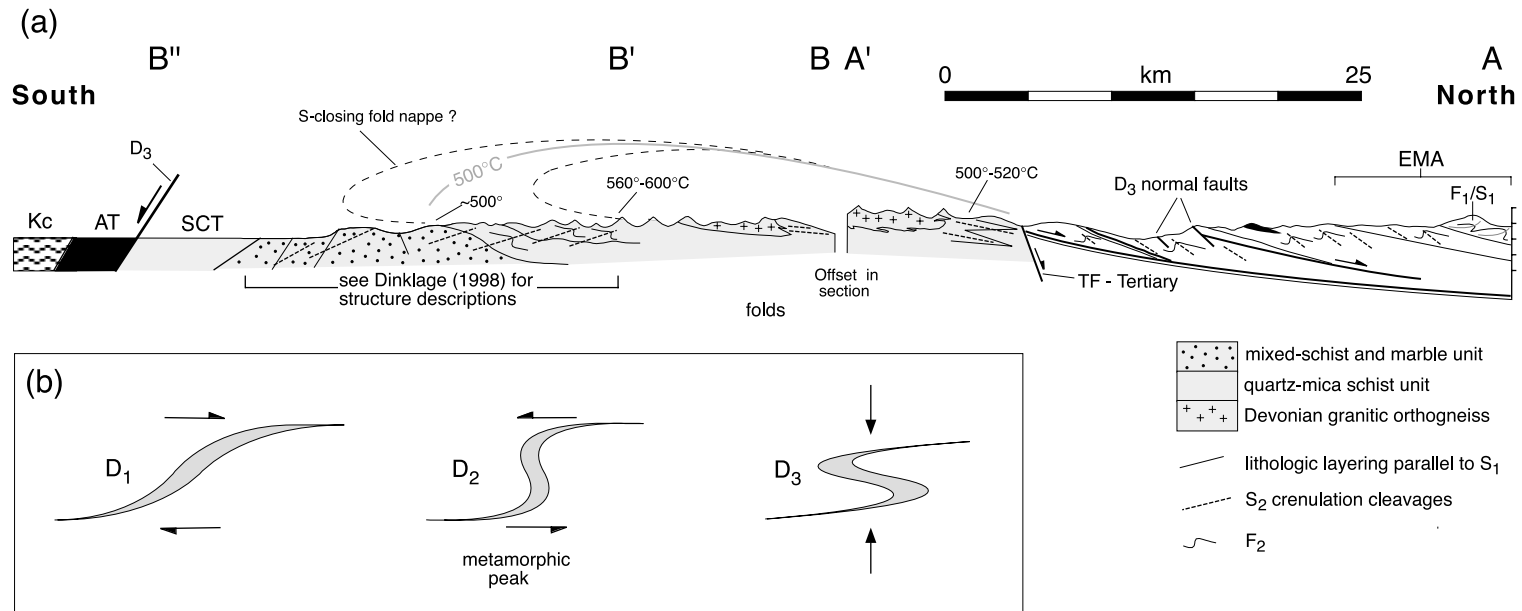


Fig. 12. (a) Cross-section across the metamorphic core showing possible regional-scale S-closing fold of mixed-schist and marble unit (black dashed lines). S_2 and regional-scale fold are interpreted to have formed during S-vergent folding, but modified greatly during subsequent D_3 horizontal extension. Minor Tertiary doming also modified the geometry. The $\sim 500^\circ\text{C}$ isotherm (gray line) approximates the extent of epidote–amphibolite–facies metamorphism. AT = Angayucham terrane, EMA = Endicott Mts. allochthon, Kc = Cretaceous clastic sedimentary rocks of the Koyokuk basin, SCT = Slate Creek terrane. Section $B'-B''$ mapped by Patrick et al. (1994) and Dinklage (1998). Remaining sections from this study. See Fig. 2 for location. (b) Simple diagram showing possible profile of inferred regional-scale S-vergent fold nappe following the three deformation events.

7. Discussion

In the following sections observations and interpretations regarding the late-orogenic structures in the study area are used to establish the spatial distribution, character, and cause of backfolding and extension on the orogen-scale, and to investigate the geodynamic setting of extension. In doing so some fundamental questions regarding orogenic processes are addressed.

7.1. Spatial distribution and character of D_2 backfolding

The distribution of asymmetric folds and S_2 cleavage geometries described here, combined with observations farther south by Dinklage (1998), may delineate a regional-scale S-closing regional fold nappe with a hinge located south of the Arrigetch Peaks orthogneiss (Figs. 12 and 13). In this interpretation, the northern upright limb of the fold nappe is defined by S-vergent folds in the greenschist-grade transition zone, and the core is defined by tight kilometer-scale folds in the epidote–amphibolite grade rocks immediately south of the Takahula Fault. In the mixed-schist and marble unit south of the Arrigetch Peaks orthogneiss, Dinklage (1998) described N-vergent folds (Fig. 12) and dominantly top-to-the-south deflections across S_2 crenulation cleavages, which are consistent with a position on the lower limb of a S-closing fold nappe. On the basis of regional lithologic juxtapositions, Mull (1978) had previously proposed that the mixed-schist and marble unit in that region was overturned, and speculated about the presence of a regionally extensive S-vergent fold nappe.

Additional evidence for overturning of the mixed-schist and marble unit south of the Arrigetch Peaks orthogneiss comes from the metamorphic-grade distribution across the southern part of the cross-section in Fig. 12. The distribution of isograds (Patrick et al., 1994; Dinklage, 1998) combined with thermobarometry (Vogl, 2000) suggest that metamorphic grade increases smoothly across N-dipping layering (Fig. 12). Patrick et al. (1994) suggested that the isograds dip northward and define an inverted gradient that formed by northward thrusting of the mixed-schist and marble unit and Devonian orthogneiss over lower grade rocks now exposed farther south. More recent metamorphic data collected by Vogl (2000), however, suggest that rocks at the northern margin of the orthogneiss were never buried more deeply than underlying rocks to the south, as required by the Patrick et al. (1994) model. Instead, the metamorphic data are more supportive of a model proposed by Dinklage (1998), where isograds dip southward and peak metamorphic conditions were reached during or after S-vergent folding, while layering was steeply inclined (Fig. 12b).

The F_2 fold styles, the strain estimates, and the lack of large-scale thrust faults all suggest that D_2 bulk strain in the transition zone was much lower than that associated with the

N-directed D_1 event. Assuming that the amount of D_2 strain and fold styles in the greenschist-grade transition zone are fairly representative of the D_2 regional strain, the regional F_2 backfolding may have involved little more than kinking of originally shallowly to moderately S-dipping layering to produce a slightly overturned forelimb on the south margin of the APO (Fig. 12b). Much of the shallowing of the overturned limb, however, may have occurred during D_3 extension (Fig. 12b), as suggested by Dinklage (1998). Although the distribution of F_2/S_2 geometries may have originally formed during large-scale D_2 backfolding, the fabrics were probably enhanced, modified, and domed during subsequent D_3 extension. Regardless of the details of fabric development, a regional fold-nappe is the best way to explain the combination of metamorphic-grade distribution, orientation of layering, and a variety of structural observations.

The relatively low strain associated with backfolding may explain why the contact zone between the Angayucham terrane and underlying metasedimentary rocks appears to have not been folded. Although the final overturning of the mixed-schist and marble unit may have occurred during D_3 extension, mapping by Dinklage (1998) has revealed steep layering farther south (Fig. 12), indicating that the southernmost part of the range may have accommodated extension differently.

D_2 appears to have not folded (or repeated by major thrust faults) the marble bands or original D_1 N-directed thrust faults. The intervening phyllites, however, are locally highly folded. The difference in behavior may reflect slight differences in orientation of layering following D_1 combined with the fact that on a bulk scale of the transition zone, D_2 may have approximated a layer-parallel shear on the upper limb of the hypothesized regional fold. Following D_1 the phyllites would be expected to have more steeply S-dipping orientations relative to D_1 N-directed thrusts and highly sheared marbles. Thus, slight S-directed movements along D_1 thrust faults and competent units such as the Noatak sandstone would have resulted in shortening of the obliquely inclined intervening phyllites (Fig. 11b).

7.2. Cause of backfolding

Backfolds and backthrusts can be found in many collisional orogens and accretionary wedges (e.g. southern Canadian Cordillera, Himalayas, Norwegian Caledonides, European Alps, Pyrenees, southern Andes). In some orogens (e.g. Pyrenees, southern Canadian Cordillera), the backfolds form early and/or throughout much of the convergent history of the orogen (e.g. Brown et al., 1986, 1993; Price, 1986; Colpron et al., 1998; Beaumont et al., 2000, and references therein). In other cases (e.g. Brooks Range, European Alps, Norwegian Caledonides), backfolds are late-orogenic, forming only after large amounts of convergence and crustal shortening (e.g. Milnes et al., 1981; Roeder, 1989; Osmundsen and Anderson, 1994; Fossen and

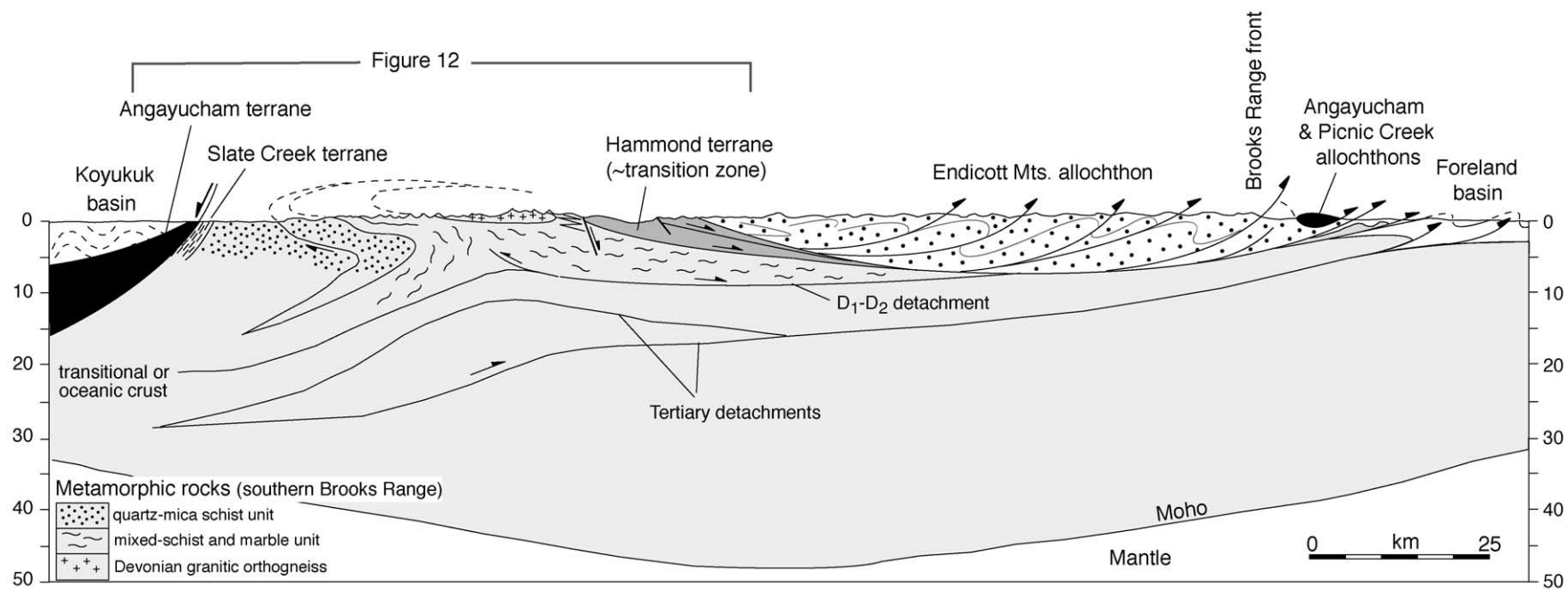


Fig. 13. Crustal-scale cross-section across central Brooks Range. Crustal thickness based on seismic images from Dalton highway Region (Fuis et al., 1995) and gravity map.

Holst, 1995; Escher and Beaumont, 1997). The onset of late-orogenic backfolding has been attributed to increased buoyancy (decrease in subductability) of the downgoing plate, which may result from the entrance of thicker continental crust into the subduction zone or from the breakoff of the oceanic lithosphere attached to downgoing continental plate (e.g. Von Blanckenburg and Davies, 1985; Beaumont et al., 1996; Escher and Beaumont, 1997).

The possibility that backfolding in the Brooks Range resulted from the entrance of thicker continental crust into the subduction zone has some merit, as revealed through examination of the crustal-scale cross-section in Fig. 13. In the cross-section, the Endicott Mountains allochthon restores to a position south of the metamorphic rocks, which is interpreted as parautochthonous pre-Devonian basement and some of its cover. The thick Devonian clastic wedge within the EMA probably records deposition in a deeper, distal part of the margin that was thinned during growth of the Angayucham ocean basin (e.g. Moore et al., 1994). Thus, restoration of this section implies that the metamorphic rocks of the southern Brooks Range represent a thicker part of the continental margin. Although the crust does become thinner over the southern third of the Brooks Range (Fuis et al., 1995), it is difficult to delineate original or post- D_1 thickness variations due to uncertainties in amount of thinning during D_3 extension and re-thickening during Tertiary contraction. On a regional scale more completely overturned limbs are found on the south margins of the larger Devonian granitic orthogneiss bodies (Arrigetch and Igikpak; Mull, 1978), suggesting that the orthogneisses may have had a local mechanical effect on the backfolding.

Another possible cause of backfolding is movement over a thrust ramp producing local antithetic structures near the ramp base ramp (Price, 1986; McClay and Buchanan, 1992; Colpron et al., 1998). Such a model was proposed by Ave Lallemand and Oldow (1998) to explain the formation of low-strain S-vergent folds near the Dalton Highway. They suggested that S-vergent folds formed from local antithetic shear during top-to-the-north thrusting and basement duplex formation in the Doonerak antiform (Fig. 1), which is believed to have formed largely in the latest Cretaceous and Tertiary (O'Sullivan et al., 1998). I do not believe that the S-vergent D_2 structures in the study area formed from the same event because: (1) structures similar to the basement duplexes in the Doonerak antiform have not been identified as far west as the study area, and (2) S-vergent structures in the study area appear to be mid-Cretaceous in age.

7.3. Spatial distribution and character of D_3 extensional strain

Late- to post-orogenic extension is a common feature of collisional orogens (e.g. Alps, Apennines, Betics, Norwegian Caledonides), as indicated by the occurrence

of normal fault systems in the hinterland regions (e.g. Carmignani and Kligfield, 1990; Steck and Hunziker, 1994; Anderson, 1998). The role that more distributed, penetrative strain, recorded by gently dipping foliations and recumbent folds (e.g. Froitzheim, 1992; Wallis et al., 1993), plays in thinning of the crust in orogenic belts, however, is less clear. Unambiguous kinematic interpretation of subhorizontal foliations and recumbent folds is problematical because they may form from a variety of strain paths, which are difficult to assess in highly recrystallized metamorphic rocks. The approach taken in this study to understanding the kinematic significance of subhorizontal foliations was to trace deep-level, higher grade fabrics into higher structural levels where kinematic histories are more easily interpreted owing to lesser amounts of recrystallization and lower strains. By tracing the variation in D_2 and D_3 structural style and documenting the porphyroblast–matrix relationships through this section, it has been concluded that the total strain recorded by recumbent folds and subhorizontal cleavages in the epidote–amphibolite facies metamorphic core probably resulted from superposed deformations (i.e. D_2 S-vergent backfolding and D_3 horizontal extension). Although these two kinematically distinct deformation events produced two identifiable sets of structures in greenschist-grade rocks, only a single relatively high-strain fabric and associated tight folds are preserved at deeper levels. Due to the inferred composite nature of the fabrics, however, the amount of D_3 extensional strain is difficult to quantify. Assignment of the post- D_1 strain recorded by the recumbent folds and S_2 cleavages in the metamorphic core entirely to either the D_2 or D_3 events would result in an overestimate of the strain associated with that event. Despite the complexities in the fabric formation, it is clear that extensional strain was not limited to normal faults on the south flank of the Brooks Range.

As discussed above, it has been inferred that ductile thinning in epidote–amphibolite facies rocks probably occurred around 103 Ma during initial cooling from the metamorphic peak and was synchronous with large-scale extensional faulting on the south flank of the range. Overall, extensional strain at ~103 Ma involved: (1) tightening of folds and associated subhorizontal S_2 crenulation cleavage development (epidote–amphibolite grade rocks), (2) small displacement (up to hundreds of meters) N-side-down displacement normal faults at higher levels on the north flank of the metamorphic culmination, and (3) large displacement (up to several kilometers) S-side-down normal faulting on the south flank of the range. Extensional strain has also been proposed by Dinkluge (1998) in the region between the Arrigetch Peaks orthogneiss and the normal faults on the south flank of the range. He suggested that extension rotated the steeply overturned limb of the proposed regional fold nappe, which produced N-side-down shearing along this N-dipping layering; he also observed S-side-down extensional shear bands and shallowly S-dipping S_2 crenulation

cleavages, which he attributed to vertical thinning. Thus, most of the southern half of the Brooks Range appears to have been affected by extension. The nature of the fabrics formed during extension appears to have been dependent on the fabric geometry following D_2 . For instance, where gently inclined folds existed, folds were tightened during D_3 extension. In other areas where layering was planar, it may have been rotated to shallow dips (Dinklage, 1998), or cut by normal faults where dips were shallow, such as at higher levels on the north flank of the culmination.

The metamorphic field gradients appear to define a thermal dome centered near the south margin of the Arrigetch Peaks orthogneiss, where peak temperatures approaching 600 °C have been estimated (Vogl, 2000; Fig. 12). South of the Arrigetch Peaks orthogneiss, S_2 crenulation cleavages dip shallowly southward (Fig. 12; Patrick et al., 1994; Dinklage, 1998), whereas S_2 dips shallowly northward to the north (this study). These crenulation cleavages are interpreted to form a structural dome that coincides spatially with the metamorphic dome. Some of the S_2 may have formed during D_2 backfolding, however, it is suggested that they were intensified during D_3 extension. Dinklage (1998) has observed S-side-down shear bands, and has suggested that S-dipping S_2 crenulation cleavages record a bulk vertical thinning with a top-to-the-south component. In contrast, on the north flank of the dome, N-side-down normal faults and shear bands have been documented. These relationships suggest doming leading to opposing shear senses on opposite flanks of the dome during D_3 extension. Thermochronologic data (Vogl et al., 2002) also suggest that doming occurred during D_3 extension beginning ca. 103 Ma. This doming was superimposed on a northward tilt caused by extensional exhumation of footwall rocks toward the southern end of the range (Vogl et al., 2002). Doming may have resulted from isostatic uplift of the footwall rocks during tectonic denudation. Mid-Cretaceous doming was probably enhanced during the Tertiary, as suggested by the southward decrease in apatite fission track ages from ~78 Ma within the Endicott Mountains allochthon to ~21–27 Ma within the Arrigetch Peaks orthogneiss (Blythe et al., 1997; Blythe and Vogl, unpublished data); limited data suggest a southward increase in ages away from the southern margin of the orthogneiss (Blythe et al., 1997).

7.4. Geodynamic setting of extension

Extension that commonly characterizes the hinterland regions of orogens may occur in a variety of geodynamic settings. Possible settings range from post-contractional rifting with lithospheric-scale extension to upper crustal extension that is synchronous with deeper level contractional structures. Furthermore, in some proposed settings, foreland thrusting is driven by hinterland extension. The different geodynamic models may be tested, in part, through delineation of the specific age relationships between

foreland thrust faults and extensional/contractional structures in the hinterland regions of orogens. In the Brooks Range, proposed models for the geodynamic setting of extension vary widely, as outlined in the introduction. These variations are the result of the lack of documentation of the kinematics and timing of late-orogenic (Aptian to Cenomanian) deformation. Our new data and proposed deformational sequence, combined with existing data provide a means to address this problem.

Above, the age of D_2 backfolding was interpreted to have slightly pre-dated initial cooling from peak metamorphic conditions at ~103 Ma, suggesting an early- to mid-Albian age (Fig. 14). Near the southern margin of the foreland basin, syndepositional folds in early- to mid-Albian deposits of the Fortress Mountain Fm. have recently been identified by Cole et al. (1997), who interpreted folding to have occurred above active thrust faults. These structures represent the youngest clearly identified contractional structures in the fold–thrust belt that are associated with Jurassic–Cretaceous orogenesis (Fig. 14; Tertiary contractional structures are widespread in the Brooks Range and its foreland basin; however, mid-Albian to latest Cretaceous contractional structures have not been identified). Thus, D_2 backfolding appears to have been synchronous with the last stages of Cretaceous (early- to mid-Albian) contraction recorded in the foreland. Furthermore, it was suggested above that the 103 Ma hornblende age represents the onset of rapid extension-related cooling, and therefore the transition from contraction (D_2 backfolding) to extension (D_3) in the metamorphic core coincided with the end of identifiable foreland thrusting. On the basis of these relationships, D_3 hinterland extension is viewed as post-orogenic and post-contractional, and is not involved as a driving mechanism for foreland thrusting in the Brooks Range, as suggested by Toro (1998). An alternative view is that the extension initiated from a slowing of convergence rates. Such a slowing could be indicated by basin modeling (Cole et al., 1997), which may suggest minor thrust-related subsidence in the foreland basin during the Late Cretaceous.

Following the theoretical model of Platt (1986), Gottschalk and Oldow (1988) suggested that along the Dalton Highway, extensional faulting was synchronous with, and a result of, deeper level contraction and thickening. The ages of the deformational events in that area, however, are poorly constrained. The applicability of the Platt (1986) model to the study area is difficult to test, because it requires that syn- to post-103 Ma contractional structures underlie the presently exposed extensional structures in the metamorphic core. Such a model would also require that thrusting did not propagate into the foreland (or is not yet identified), but was rather manifested as a deep crustal wedge.

7.5. Implications for evolution of flanking sedimentary basins

The northern lobe of the Koyukuk basin (Figs. 1, 12 and

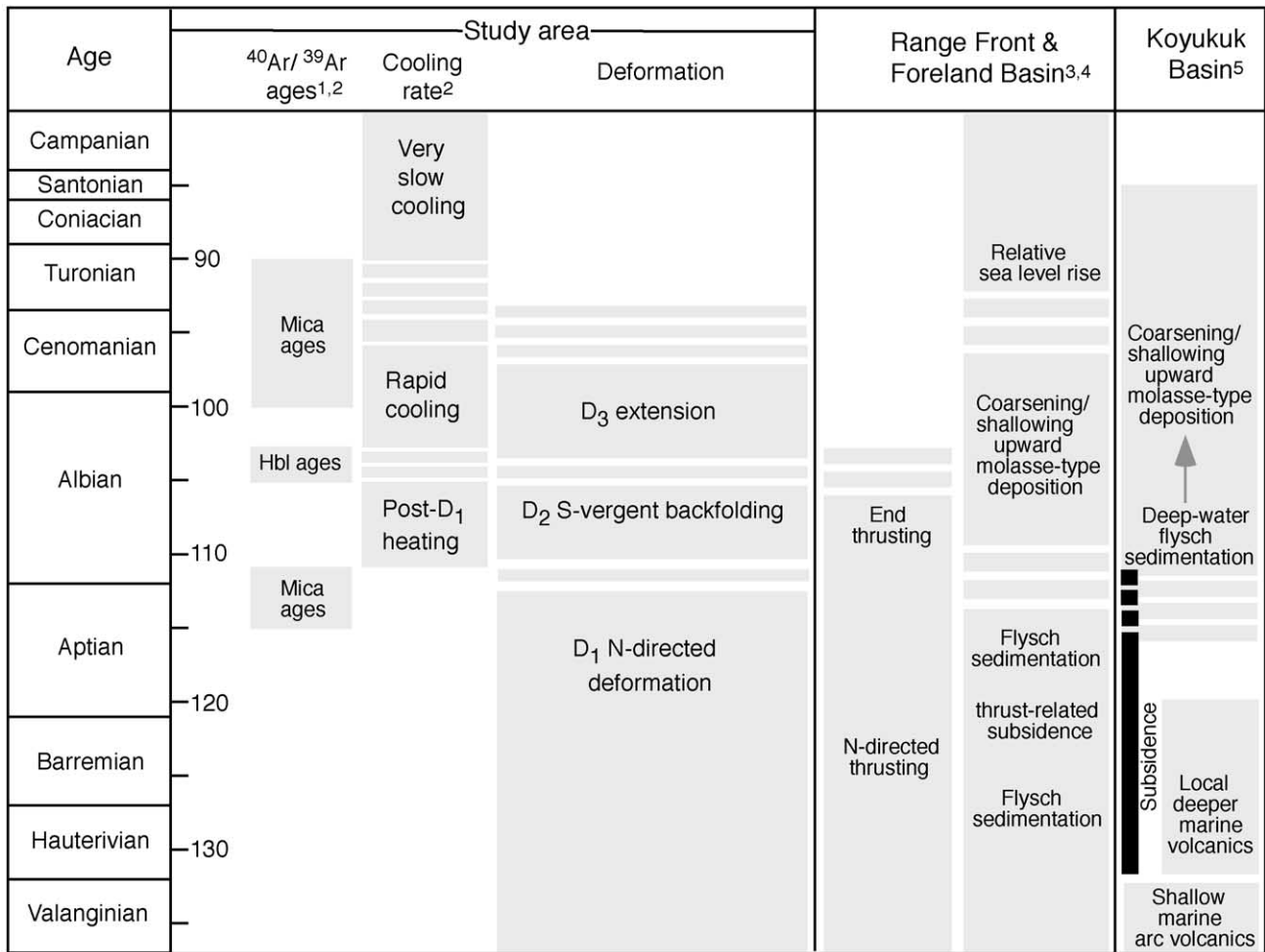


Fig. 14. Summary of ages of geological events in the study area and flanking sedimentary basins. References: 1 = Toro, 1998; 2 = Vogl et al., 2002; 3 = Mull, 1985; 4 = Cole et al., 1997; 5 = Nilsen, 1989.

13) lies between the Brooks Range and volcanic/intrusive rocks of the Koyukuk terrane, which is believed to represent an intra-oceanic island arc (e.g. Patton and Box, 1989). The basin is filled with an Albian to Santonian flysch-to-molasse sequence up to ~4 km thick (Nilsen, 1989). On the southern margin of the basin, the early Albian deep-water flysch in the Koyukuk basin overlies Valanginian shallow-water island-arc volcanogenic strata, indicating significant Hauterivian to early Albian subsidence south of the Brooks Range (Fig. 14; Nilsen, 1989). The clast compositions in the sedimentary sequence appear to record unroofing of progressively deeper levels of the adjacent Brooks Range orogen (e.g. Dillon, 1989). The relationship between the structural history of the Brooks Range and evolution of the Koyukuk basin has not been clearly established.

Miller and Hudson (1991) suggested that subsidence and unroofing recorded in the Koyukuk basin are the result of post-Valanginian (130–90 Ma) lithospheric-scale extension. The deformational sequence interpreted here, however, involves contractional deformation (D₂ backfolding) as young as Albian, overlapping with sedimentation in

the basin, and well into the period of extension proposed by Miller and Hudson (1991). Furthermore, Vogl et al. (2002) show that the dominant period of cooling and exhumation began around 103 Ma, well after the dominant period of subsidence in the Koyukuk basin. These data and interpretations suggest that the subsidence and subsequent unroofing recorded in the Koyukuk basin are not easily correlated with a simple prolonged extensional event. If our interpreted deformational sequence is correct, then the Albian and younger flysch–molasse sequence in the Koyukuk basin must have accumulated during both backfolding and extension. The cause of the Hauterivian to early Albian subsidence in the Koyukuk basin is difficult to directly evaluate because the basin margins have complicated structural histories involving thrust, normal and strike-slip faulting, all of which are poorly constrained in terms of age. Finally, it is noted that basins with similarly unclear subsidence mechanisms in analogous settings occur in the Banda arc and Taiwan arc-continent collision zones (e.g. Milsom and Audley-Charles, 1986; Karig et al., 1987; Dorsey, 1992).

8. Concluding remarks

Previous work in the southern Brooks Range has not satisfactorily documented the late-orogenic kinematic history, leading to widely varying models for the orogen-scale evolution of the Brooks Range. Combined with $^{40}\text{Ar}/^{39}\text{Ar}$ data, new structural observations from a range of crustal levels suggest that the well-documented protracted phase of Early Cretaceous N-directed D_1 deformation was followed by early- to mid-Albian backfolding (D_2) and mid-Albian to Cenomanian extension (D_3). The observations and interpretations, provide new insights into the much-debated late-orogenic evolution of the Brooks Range. Furthermore, the conclusions allow assessment of the character and timing of backfolding and extension across the orogen, as well as investigation of the geodynamic development during collision. Therefore, given the common occurrence of backfolding and extension in collisional orogens, the conclusions are of relevance to orogenic processes. Some of the salient conclusions that are of general relevance are as follows.

The final stages of contraction involved apparently synchronous D_2 backfolding toward the rear of the orogen and northward thrusting near the range front. There is no evidence that the main extensional event beginning around 103 Ma overlapped with contraction in either the foreland or hinterland, suggesting that hinterland extension was post-contractional and did not drive foreland thrusting.

Extensional strain, although locally low in magnitude, affected much of the southern Brooks Range and was manifested in various ways including large- and small-displacement normal faults, shearing along layer-parallel foliations, and tightening of previously formed folds. The extensional structural style was probably dependent on pre-extensional fabric geometry. Within lowermost-amphibolite facies rocks of the study area, the initiation of folds during D_2 backfolding may have allowed subsequent D_3 extensional deformation to occur through tightening of F_2 folds and associated S_2 crenulation cleavage development, leaving only a single high-strain composite D_2 – D_3 fabric that is axial-planar to tight recumbent folds in the metamorphic core. Such a kinematic history may provide a general explanation for the common occurrence of subhorizontal foliations and recumbent folds deep levels of orogens, and some core complexes in particular, which typically show evidence for contractional deformation followed by extension.

Acknowledgements

This work is part of the authors Ph.D. dissertation at University of California—Santa Barbara. The research was funded by National Science Foundation grant EAR-9405560, awarded to Brian Patrick and Bill McClelland. Other funding was provided by the Geological Society of

America and Sigma Xi. I thank the National Park Service for allowing access into Gates of the Arctic National Park. I gratefully acknowledge Lindsay Maw, Donovan Stevens, Matt Nyman, Libby Gans, Eric Vanek, and Todd Gardiner for assistance in the field. Many thanks to Brian Patrick for the introduction to Brooks Range geology, and A. Blythe, W. Dinklage, T. Moore G. Mull, M. Nyman and W. Wallace for helpful scientific discussions. The paper benefited greatly from thorough reviews by W. Wallace and E. Miller. Thanks to W. McClelland and P. Gans for reviewing early versions of the manuscript.

References

- Adams, K.E., Mull, C.G., Crowder, R.K., 1997. Permian deposition in the north central Brooks Range, Alaska: constraints for tectonic reconstructions. *Journal of Geophysical Research* 102, 20,727–20,748.
- Anderson, T.B., 1998. Extensional tectonics in the Caledonides of southern Norway, an overview. *Tectonophysics* 285, 333–351.
- Armstrong, R.L., Harakal, J.E., Forbes, R.B., Evans, B.W., Thurston, S.P., 1986. Rb–Sr and K–Ar study of metamorphic rocks of the Seward Peninsula and Southern Brooks Range, Alaska. In: Evans, B.W., Brown, E.H. (Eds.), *Blueschists and Eclogites*. Geological Society of America Memoir 164, pp. 185–203.
- Ave Lallemand, H.G., Oldow, J.S., 1998. Antithetic shear and the formation of backfolds in the central Brooks Range fold and thrust belt, Alaska. In: Oldow, J.S., Ave Lallemand, H.G. (Eds.), *Architecture of the Central Brooks Range Fold and Thrust Belt, Arctic Alaska*. Geological Society of America Special Paper 324, pp. 253–259.
- Beaumont, C., Ellis, S., Hamilton, J., Fullsack, P., 1996. Mechanical model for subduction–collision tectonics of Alpine-type compressional orogens. *Geology* 24, 675–678.
- Beaumont, C., Munoz, J.A., Hamilton, J., Fullsack, P., 2000. Factors controlling the Alpine evolution of the central Pyrenees inferred from a comparison of observations and geodynamical models. *Journal of Geophysical Research* 105, 8121–8145.
- Blythe, A.E., Murphy, J., O’Sullivan, P.B., 1997. Tertiary cooling and deformation in the south-central Brooks Range: evidence from zircon and apatite fission-track analyses. *Journal of Geology* 105, 583–599.
- Brown, R.L., Journeay, M.J., Lane, L.S., Murphy, D.C., Rees, C.J., 1986. Obduction, backfolding, and piggyback thrusting in the metamorphic hinterland of the southeastern Canadian Cordillera. *Journal of Structural Geology* 8, 255–268.
- Brown, R.L., Beaumont, C., Willet, S.D., 1993. Comparison of the Selkirk fan structure with mechanical models: implications for interpretation of the southern Canadian Cordillera. *Geology* 21, 1015–1018.
- Carlson, C., 1985. Large-scale, south-dipping low-angle normal faults in the southern Brooks Range, Alaska. *Eos, Transactions AGU* 66, 1074.
- Carmignani, L., Kligfield, R., 1990. Crustal extension in the Northern Apennines: the transition from compression to extension in the Alpi Apuane Core Complex. *Tectonics* 9, 1275–1304.
- Christiansen, P.P., Snee, L.W., 1994. Structure, metamorphism, and geochronology of the Cosmos Hills and Ruby Ridge, Brooks Range schist belt, Alaska. *Tectonics* 13, 193–213.
- Cole, F., Bird, K.J., Toro, J., Roure, F., O’Sullivan, P.B., Pawlewicz, M., Howel, D.G., 1997. An integrated model for the tectonic development of the frontal Brooks Range and Colville Basin 250 km west of the trans-Alaska Crustal Transect. *Journal of Geophysical Research* 102, 20,685–20,708.
- Colpron, M., Warren, M.J., Price, R.A., 1998. Selkirk fan structure, southeastern Canadian Cordillera: Tectonic wedging against an inherited basement ramp. *Geological Society of America Bulletin* 110, 1060–1074.

- Davis, D., Suppe, J., Dahlen, F.A., 1983. Mechanics of fold-and-thrust belts and accretionary wedges. *Journal of Geophysical Research* 88, 1153–1172.
- Dewey, J.F., 1988. Extensional collapse of orogens. *Tectonics* 7, 1123–1139.
- Dillon, J.T., 1989. Structure and stratigraphy of the southern Brooks Range and northern Koyukuk basin near the Dalton Highway. In: Mull, C.G., Adams, K.E. (Eds.), *Dalton Highway, Yukon River to Prudhoe Bay, Alaska, Bedrock Geology of the Eastern Koyukuk basin, Central Brooks Range, and East-central Arctic Slope*. Alaska Division of Geological and Geophysical Surveys, pp. 157–188.
- Dinklage, W.S., 1998. Extension of a convergent orogen: structural evolution of the high-pressure/low-temperature schist belt, Brooks Range, Alaska. Ph.D. Thesis. University of California, Santa Barbara.
- Dorsey, R.J., 1992. Collapse of the Luzon volcanic arc during onset of arc-continent collision: evidence from a miocene–pliocene unconformity, eastern Taiwan. *Tectonics* 11, 177–191.
- Dusel-Bacon, C., Brosge, W.P., Till, A.B., Mayfield, C.F., Reiser, H.N., Miller, T.P., 1989. Distribution, facies, ages and proposed tectonic associations of regionally metamorphosed rocks in northern Alaska, U.S. Geological Survey Professional Paper 1497A.
- Escher, A., Masson, H., Steck, A., 1993. Nappe geometry in the Western Swiss Alps. *Journal of Structural Geology* 15, 501–509.
- Escher, A., Beaumont, C., 1997. Formation, burial, and exhumation of basement nappes at crustal scale: a geometric model based on the Western Swiss–Italian Alps. *Journal of Structural Geology* 7, 955–974.
- Estabrook, C.H., Stone, D.B., Davies, J.N., 1988. Seismotectonics of Northern Alaska. *Journal of Geophysical Research* 93, 12,026–12,040.
- Fossen, H., Holst, T.B., 1995. Northwest-verging folds and the north-westward movement of the Caledonian Jotun Nappe, Norway. *Journal of Structural Geology* 17, 3–15.
- Froitzheim, N., 1992. Formation of recumbent folds during synorogenic crustal extension (Austroalpine nappes, Switzerland). *Geology* 20, 923–926.
- Fuis, G.S., Levander, A.R., Lutter, W.J., Wissinger, E.S., Moore, T.E., Christensen, N.I., 1995. Seismic images of the Brooks Range, Arctic Alaska, reveal crustal-scale duplexing. *Geology* 23, 65–68.
- Gottschalk, R.R., Oldow, J.S., 1988. Low-angle normal faults in the south-central Brooks Range fold and thrust belt, Alaska. *Geology* 16, 395–399.
- Gottschalk, R.R., Oldow, J.S., Ave Lallemand, H.G., 1998. Geology and Mesozoic structural history of the south-central Brooks Range, Alaska. In: Oldow, J.S., Ave Lallemand, H.G. (Eds.), *Architecture of the Central Brooks Range Fold and Thrust Belt, Arctic Alaska*. Geological Society of America Special Paper 324, pp. 195–223.
- Gutscher, M.-A., Kukowski, N., Malavieille, J., Lallemond, S., 1996. Cyclical behavior of thrust wedges: insights from high basal friction experiments. *Geology* 24, 135–138.
- Gutscher, M.-A., Kukowski, N., Malavieille, J., Lallemond, S., 1998. Material transfer in accretionary wedges from analysis of a systematic series of analog experiments. *Journal of Structural Geology* 20, 407–416.
- Handschy, J.W., 1998. Spatial variation in structural style, Endicott Mountains allochthon, central Brooks Range, Alaska. In: Oldow, J.S., Ave Lallemand, H.G. (Eds.), *Architecture of the Central Brooks Range Fold and Thrust Belt, Arctic Alaska*. Geological Society of America Special Paper 324, pp. 33–50.
- Hammer, S., Passchier, C., 1991. Shear-sense indicators: a review. *Geological Survey of Canada, Paper*, 90-12, 71pp.
- Karig, D.E., Barber, A.J., Charlton, T.R., Klemperer, S., Hussong, D.M., 1987. Nature and distribution of deformation across the Banda Arc–Australian collision zone at Timor. *Geological Society of America Bulletin* 98, 18–32.
- Koons, P.O., 1990. Two-sided orogen: collision and erosion from the sand-box to the Southern Alps, New Zealand. *Geology* 18, 679–682.
- Krabbendam, M., Leslie, A.G., 1996. Folds with vergence opposite to the sense of shear. *Journal of Structural Geology* 18, 777–781.
- Law, R.D., Miller, E.M., Little, T.A., Lee, J., 1994. Extensional origin of ductile fabrics in the Schist Belt, Central Brooks Range, Alaska—II. Microstructural and petrofabric evidence. *Journal of Structural Geology* 16, 919–940.
- Little, T.A., Miller, E.M., Lee, J., Law, R.D., 1994. Extensional origin of ductile fabrics in the Schist Belt, Central Brooks Range, Alaska—I. Geologic and structural studies. *Journal of Structural Geology* 16, 899–919.
- Malavieille, J., 1993. Late orogenic extension in mountain belts: insights from the basin and range and the Late Paleozoic Variscan belt. *Tectonics* 12, 1115–1130.
- Mayfield, C.F., TAILLEUR, I.L., ELLERSIECK, I., 1988. Stratigraphy, structure and palinspastic synthesis of the western Brooks Range, northwestern Alaska. In: Gryc, G. (Ed.), *Geology and Exploration of the National Petroleum Reserve in Alaska 1974–1982*. U.S. Geological Survey Professional Paper 1399, pp. 143–186.
- McClay, K.R., Buchanan, P.G., 1992. Thrust faults in inverted extensional basins. In: McClay, K.R. (Ed.), *Thrust Tectonics*. New York, Chapman & Hall, pp. 93–104.
- Miller, E.L., Hudson, T.L., 1991. Mid-Cretaceous extensional fragmentation of a Jurassic–Early Cretaceous compressional orogen. *Tectonics* 10, 781–796.
- Milnes, A.G., Grellier, M., Muller, R., 1981. Sequence and style of major post-nappe structures, Simplon–Pennine Alps. *Journal of Structural Geology* 3, 411–420.
- Milsom, J., Audley-Charles, M.G., 1986. Post-collision isostatic readjustment in the southern Banda Arc. In: Coward, M.P., Ries, A.C. (Eds.) *Collision Tectonics*, Geological Society of London Special Publication 19, pp. 353–364.
- Moore, T.E., Wallace, W.K., Bird, K.J., Karl, S.M., Mull, C.G., Dillon, J.T., 1994. Geology of northern Alaska. In: Plafker, G., Berg, H.C. (Eds.), *The Geology of North America, vol. G-1, The Geology of Alaska*. Geological Society of America, pp. 49–140.
- Moore, T.E., Wallace, W.K., Mull, C.G., Adams, K.E., Plafker, G., Nokleberg, W.J., 1997. Crustal implications of bedrock geology along the Trans-Alaska Crustal Transect (TACT) in the Brooks Range, northern Alaska. *Journal of Geophysical Research* 102, 20,645–20,684.
- Mull, C.G., 1978. Apparent south vergent folding and possible nappes in the Schwatka Mountains. U.S. Geological Survey Circular 751-B, B29–B31.
- Mull, C.G., 1982. Tectonic evolution and structural style of the Brooks Range, Alaska: an illustrated summary. In: Blake, R.B. (Ed.), *Geologic Studies of the Cordilleran Thrust Belt*. Rocky Mountain Association of Geologists, pp. 1–45.
- Mull, C.G., 1985. Cretaceous tectonics, depositional cycles, and the Nanushuk Group, Brooks Range and Arctic Slope, Alaska. In: Huffman, A.C., Jr. (Ed.), *Geology of the Nanushuk Group and Related Rocks, North Slope, Alaska*. U.S. Geological Survey Bulletin 1614, pp. 7–36.
- Mull, C.G., Adams, K.E., Dillon, J.T., 1989. Stratigraphy and structure of the Doonerak Fenster and Endicott Mountains allochthon, central Brooks Range. In: Mull, C.G., Adams, K.E. (Eds.), *Dalton Highway, Yukon River to Prudhoe Bay, Alaska, Bedrock Geology of the Eastern Koyukuk basin, Central Brooks Range, and East-central Arctic Slope*. Alaska Division of Geological and Geophysical Surveys, pp. 203–217.
- Nelson, S.W., Grybeck, D., 1980. Geologic map of the Survey Pass quadrangle, Brooks Range, Alaska. U.S. Geological Survey, Miscellaneous Field Studies, MF-1176, scale 1:250,000.
- Nelson, S.W., Grybeck, D., 1981. Map showing distribution of metamorphic rocks in the Survey Pass quadrangle, Brooks Range, Alaska. U.S. Geological Survey, Miscellaneous Field Studies, MF-1176-C1, scale 1:250,000.
- Nilsen, T.H., 1989. Stratigraphy and sedimentology of mid-Cretaceous deposits of the Yukon–Koyukuk Basin, west central Alaska. *Journal of Geophysical Research* 94, 15,925–15,940.

- Oldow, J.S., Seidensticker, C.M., Phelps, J.C.J., Gottschalk, R.R., Boler, K.W., Handschy, J.W., Ave Lallemand, H.G., 1987. Balanced cross-sections through the central Brooks Range and North Slope, arctic Alaska. *American Association of Petroleum Geologists*, 19pp. 8 plates.
- Osmundsen, P.T., Anderson, T.B., 1994. Caledonian compressional and late-orogenic extensional deformation in the Stavenest area, Sunnfjord, Western Norway. *Journal of Structural Geology* 16, 1385–1401.
- O'Sullivan, P.B., Hanks, C.L., Wallace, W.K., Green, P.F., 1995. Multiple episodes of Cenozoic denudation in the northeastern Brooks Range: fission-track data from the Okpilak batholith, Alaska. *Canadian Journal of Earth Sciences* 32, 1106–1118.
- O'Sullivan, P.B., Moore, T.E., Murphy, J.M., 1998. Tertiary uplift of the Mt. Doonerak antiform, central Brooks Range, Alaska: apatite fission-track evidence from the trans-Alaska crustal transect. In: Oldow, J.S., Ave Lallemand, H.G. (Eds.), *Architecture of the Central Brooks Range Fold and Thrust Belt, Arctic Alaska*. Geological Society of America Special Paper 324, pp. 179–193.
- Parrish, R.R., Carr, S.D., Parkinson, D.L., 1988. Eocene extensional tectonics and the geochronology of the southern Omenica belt, British Columbia. *Tectonics* 7, 181–212.
- Patrick, B., Till, A.B., Dinklage, W.S., 1994. An inverted metamorphic field gradient in the central Brooks Range, Alaska and implications for exhumation of high-pressure/low-temperature metamorphic rocks. *Lithos* 33, 67–83.
- Patton, W.W., Box, S.E., 1989. Tectonic setting of the Yukon–Koyukuk Basin and its borderlands, Western Alaska. *Journal of Geophysical Research* 94, 15,807–15,820.
- Platt, J.P., 1986. Dynamics of orogenic wedges and uplift of high-pressure metamorphic rocks. *Geological Society of America Bulletin* 97, 1037–1053.
- Platt, J.P., Vissers, R.L.M., 1980. Extensional structures in anisotropic rocks. *Journal of Structural Geology* 2, 397–410.
- Price, R.A., 1986. The southeastern Canadian Cordillera: thrust faulting, tectonic wedging, and delamination of the lithosphere. *Journal of Structural Geology* 8, 239–254.
- Ramsay, J.G., 1967. *The Folding and Fracturing of Rocks*. McGraw Hill Book Company, New York 568pp.
- Ramsay, R.G., Casey, M., Kligfield, R., 1983. Role of shear in development of the Helvetic fold–thrust belt of Switzerland. *Geology* 11, 439–442.
- Roeder, D., 1989. South-Alpine thrusting and trans-Alpine convergence. In: Coward, M.P., Dietrich, D., Park, R.G. (Eds.), *Alpine Tectonics*, Geological Society of London Special Publication 45, pp. 47–63.
- Steck, A., Hunziker, J., 1994. The Tertiary structural and thermal evolution of the Central Alps—compressional and extensional structures in an orogenic belt. *Tectonophysics* 238, 229–254.
- Stockmal, G.S., 1983. Modeling of large-scale accretionary wedge deformation. *Journal of Geophysical Research* 88, 8271–8287.
- Toro, J., 1998. Structure and thermochronology of the metamorphic core of the Brooks Range, Alaska. Ph.D. Thesis, Stanford University.
- Turner, D.L., Forbes, R.B., Dillon, J.T., 1979. K–Ar geochronology of the southwestern Brooks Range, Alaska. *Canadian Journal of Earth Sciences* 16, 1789–1804.
- Vogl, J.J., 2000. Tectono-thermal evolution of the Brooks Range collisional orogen, Alaska: insights from a structural, metamorphic, and $^{40}\text{Ar}/^{39}\text{Ar}$ thermochronology study of the Arrigetch Peaks region. Ph.D. Thesis, University of California, Santa Barbara.
- Vogl, J.J., Gans, P.B., Calvert, A.T., 2002. Mechanisms and timing of exhumation of collision-related metamorphic rocks southern Brooks Range, Alaska: insights from $^{40}\text{Ar}/^{39}\text{Ar}$ thermochronology. Submitted to *Tectonics*, in review.
- Von Blanckenburg, F., Davies, J.H., 1985. Slab breakoff: a model for syncollisional magmatism and tectonics in the Alps. *Tectonics* 14, 120–131.
- Wallis, S.R., Platt, J.P., Knott, S.D., 1993. Recognition of syn-convergence extension in accretionary wedges with examples from the Calabrian arc and the Eastern Alps. *American Journal of Science* 293, 463–495.
- Wirth, K.R., Bird, J.M., Blythe, A.E., Harding, D.J., 1993. Age and evolution of western Brooks Range ophiolites Alaska: results from $^{40}\text{Ar}/^{39}\text{Ar}$ thermochronometry. *Tectonics* 12, 410–432.